FOCUS REVIEW

Electrochemical Materials and Technologies

eISSN: 2949-0561

Cite this: Electrochem. Mater. Technol. 2 (2023) 20232025

Short review on recent studies and prospects of application of rare-earth-doped $La_2NiO_{4+\delta}$ as air electrodes for solid-oxide electrochemical cells

Elena Pikalova [a], Ekaterina Guseva [b], Elena Filonova [b]*

Received: 16 October 2023
Accepted: 2 November 2023
Published online: 14 November 2023

DOI: 10.15826/elmattech.2023.2.025

Solid solutions based on the rare earth substituted lanthanum nickelate $La_2NiO_{4+\delta}$ are considered as promising air electrode materials for electrochemical applications. The present focus review summarizes recently published papers dealing with synthesis methods and investigations of the crystal structure, physicochemical properties, oxygen diffusion and electrochemical activity of $La_{2-x}Ln_xNiO_{4+\delta}$ (Ln = Pr, Nd, Sm, Eu, Gd) electrode materials. It highlights the application advantages and drawbacks of the Ln-substituted $La_2NiO_{4+\delta}$ for solid oxide fuel and electrolysis cells and compared to the non-substituted $La_2NiO_{4+\delta}$.

keywords: solid oxide fuel cells, air electrode, Ruddlesden – Popper phases, lanthanum nickelate, rare-earth element

1. Introduction

Ruddlesden – Popper (RP) phases of the first order [1, 2], represented, particularly, by $Ln_2NiO_{4+\delta}$ (Ln = rare earth element, REE) complex oxides, are considered by materials scientists to be promising electrode materials for solid oxide fuel and electrolysis cells (SOFCs and SOECs) [3–8]. They have a layered structure, which determines both the presence of mixed conductivity and high oxygen mobility [9, 10], as well as the possibility of wide variation in the chemical composition [6, 11–14]. Layered nickelates have been attracting more and more attention from the Russian scientific community as well. At present, the most numerous publications are devoted to the study of functional properties of $La_2NiO_{4+\delta}$-based solid solutions and various aspects of their electrochemical application in the cells with both oxygen ion and proton-conducting electrolytes [15–25].

Currently, it has been shown that doping $La_2NiO_{4+\delta}$ at the A-site with alkali-earth elements contributes to an increase in the overall electrical conductivity, but at the same time decreases the content of highly mobile interstitial oxygen, which may deteriorate oxygen diffusion and electrode performance [26–30]. In addition, the segregation phenomenon of alkaline earth ions on the surface of the working electrode leads to the blocking of oxygen access to the catalytic surface, which causes the degradation of fuel cell capacity during long-term operation [31–33]. A possible way to preserve the high content of excess oxygen in the studied materials, which is responsible for the fast kinetics of the oxygen reduction reaction, is the substitution of a part of the lanthanum ions in $La_2NiO_{4+\delta}$ by the REE ions Ln = Pr, Nd, Sm, Eu, Gd [34, 35]. With a decrease in the average ionic radius of the cation at the A-site, a related reduction in the migration barrier of oxygen ions is expected with a minimal value

a: Institute of High-Temperature Electrochemistry UB RAS, Yekaterinburg 620066, Russia
b: Institute of Natural Sciences and Mathematics, Ural Federal University, Yekaterinburg 620002, Russia

* Corresponding author: elena.filonova@urfu.ru

attained for Gd, predicted using theory and first-principles calculations by Li et al. [36].

The optimal choice of the REE substituent ion when doping lanthanum in $La_2NiO_{4+\delta}$ can solve the problem of long-term stability of the electrochemical cell by improving the chemical and mechano-thermal electrode / electrolyte compatibility with preservation of electrochemical activity of the electrode. Doping with REE is relatively new and has perspectives for development. Therefore, the aim of the present work is to overview existing studies on preparation methods, crystal structure, oxygen diffusion, functional properties, and electrochemical performance of $La_{2-x}Ln_xNiO_{4+\delta}$ complex oxides and their evaluation as possible air electrode materials.

2. Short view on synthesis methods, crystal structure and functional properties of $La_2NiO_{4+\delta}$

$La_2NiO_{4+\delta}$ complex oxide belongs to a series of first order Ruddlesden – Popper phases ($n = 1$) [37], schematically shown in Figure 1a. It can crystallize in the orthorhombic or tetragonal structure type depending on the synthesis method and the final synthesis temperature, which determine the value of the oxygen over-stoichiometry. The schematic image of the $La_2NiO_{4+\delta}$ unit cell, presenting the alteration of the perovskite and rock-salt layers, is shown in Figure 1b. Table 1 summarizes the literature data with values of unit cell parameters illustrating the influence of the synthesis method and the final annealing temperature on the crystal structure of $La_2NiO_{4+\delta}$. Flura et al. [38] have constructed a phase diagram of $La_2NiO_{4+\delta}$, and stated that the boundary between the two phase domains (the existence of the tetragonal phase *I4/mmm* and the orthorhombic phase *Fmmm*) lies in the range of oxygen content $0.11 < \delta < 0.15$. The study of the oxygen non-stoichiometry of $La_2NiO_{4+\delta}$ performed in [26, 34, 39, 40] showed that the oxide with orthorhombic structure has values of the absolute oxygen non-stoichiometry δ equal to 0.17, 0.15, 0.18, and 0.18, respectively. The sample with the tetragonal structure was characterized by lower values of the absolute oxygen non-stoichiometry: $\delta = 0.08$ according to [41] and $\delta = 0.13$ according to [42], which is in general agreement with the phase diagram constructed in [38]. Jorgensen et al. [40] noted that stoichiometric La_2NiO_4 crystallizes in the orthorhombic space group *Bmab*. In the intergrowth RP structure of $La_2NiO_{4+\delta}$, built of alternating perovskite like

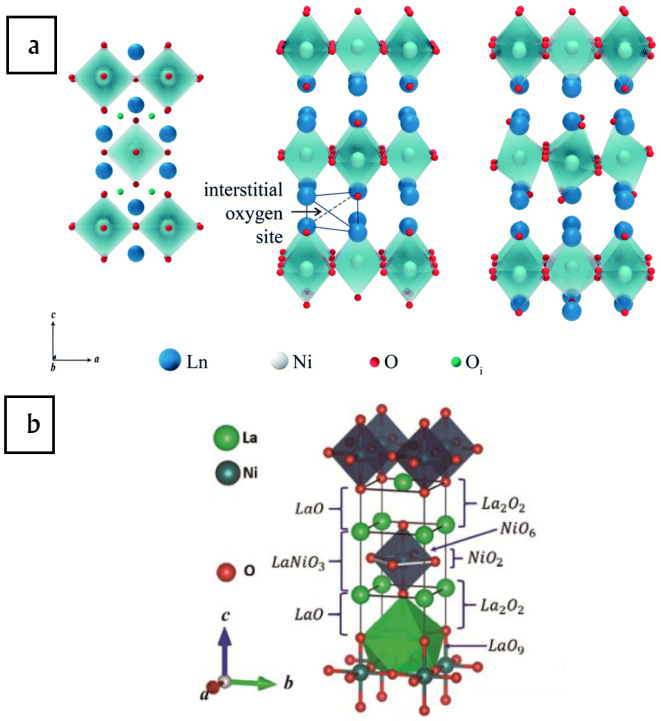

Figure 1 Schemes of possible crystal structures of Ruddlesden – Popper phases $Ln_{n+1}Ni_nO_{3n+1}$ ($n = 1$): tetragonal (center) and orthorhombic (right) (a); Schematic image of the $La_2NiO_{4+\delta}$ unit cell (b) ((a) is reproduced from [15]; (b) is reproduced from [1]).

Table 1 – Unit cell parameters of the complex oxide $La_2NiO_{4+\delta}$ obtained by different synthesis methods.

Space group	*a*, Å	*b*, Å	*c*, Å	Synthesis method, final annealing temperature, °C	Ref.
I4/mmm	3.8662(1)	3.8662(1)	12.6890(4)	Formate pyrolysis	[42]
	3.8625(1)	3.8625(1)	12.6916(4)	Combustion of glycine-nitrate compositions, 1100	[41]
Fmmm	5.4532(2)	5.4686(2)	12.6764(5)	Combustion of citrate-nitrate compositions, 1000	[43]
	5.4499(3)	5.4574(3)	12.6724(5)	Combustion of citrate-nitrate compositions, 950	[44]
	5.4628(4)	5.4664(4)	12.6827(4)	Combustion of organic-nitrate compositions, 1150	[26]
	5.458(9)	5.462(7)	12.689(2)	Electrostatic atomization method, 950	[45]
	5.4585(1)	5.4648(1)	12.6865(1)	Combustion of glycerol-nitrate compositions, 1200	[8]
	5.4482(1)	5.4773(4)	12.6668(8)	Solid-state reaction method	[46]
Bmab	5.4722	5.4772	12.6259	Combustion of citrate-nitrate compositions, 1200 (nitrogen atmosphere)	[38]

Table 2 – Oxygen self-diffusion coefficient values for $La_2NiO_{4+\delta}$.

D^*, 700 °C, $cm^2 \cdot s^{-1}$	E_D, kJ · mol^{-1}	Method	Ref.
$3.38 \cdot 10^{-8}$	82	SIMS[a]/IEDP[b]	[44]
$3.38 \cdot 10^{-8}$	82	SIMS/IEDP	[51]
$1.0 \cdot 10^{-8}$	130	IE $^{18}O_2$[c]	[46]
$1.0 \cdot 10^{-8}$	130	IE $^{18}O_2$	[52]
$2.0 \cdot 10^{-9}$	100	TPIE $C^{18}O_2$[d]	[26]
$5.5 \cdot 10^{-10}$	100	TPIE $C^{18}O_2$	[53]
$8.7 \cdot 10^{-10}$	100	TPIE $C^{18}O_2$	[34]

[a] – Secondary Ion Mass Spectrometry;
[b] – Isotope Exchange Depth Profile;
[c] – Isotope Exchange with gas phase equilibration;
[d] – Temperature-programmed Isotope Exchange of oxygen with $O^{18}O_2$.

Table 3 – TEC values for $La_2NiO_{4+\delta}$ and some electrolytes.

Material	TEC · 10^6, K^{-1}	Ref.
$La_2NiO_{4+\delta}$	13	[57]
	14.5	[42]
	13.2	[58]
	13.1	[59]
$Ce_{0.8}Gd_{0.2}O_{1.9}$	12.2	[42]
	12.3	[60]
$Ce_{0.8}Sm_{0.2}O_{1.9}$	12	[60]
$La_{0.9}Sr_{0.1}Ga_{0.8}Mg_{0.2}O_{2.85}$	12	[61]
8YSZ (92 % ZrO_2 – 8 % Y_2O_3)	10.4	[38]
$La_{10-x}Si_{6-y}Al_yO_{27-3x/2-y/2}$	8.7–10.8	[62]
$BaCe_{0.89}Gd_{0.1}Cu_{0.01}O_3$	10.5 (50–600) 8.6 (600–900)	[63]
$BaZr_{0.8}Y_{0.2}O_{3-\delta}$	8.2	[59]
$La_{1-x}Ca(Sr)_xScO_{3-\alpha}$	8.5–8.7	[64]

and rock-salt layers, oxygen anions can diffuse via the vacancy and interstitial migration mechanisms, respectively. Two-dimensional electronic transport occurs predominantly in $LaNiO_3$ perovskite layers, while La_2O_2 rock-salt type layers govern oxygen interstitial migration. Despite of the migration energy value for oxygen ion transport in the $La_2NiO_{4+\delta}$ perovskite-like layers (~0.6 eV [47] is similar or even lower than those for perovskite phases, it was shown theoretically that the relevant mechanisms describing oxygen migration in $La_2NiO_{4+\delta}$ are more complicated than those in perovskite-type oxides, and involve cooperative movements of both regular and highly mobile interstitial oxygen ions through a cooperative mechanism (an interstitialcy mechanism) [9, 48, 49]. Such the feature of oxygen transport provides for $La_2NiO_{4+\delta}$ the high values of the coefficients of chemical diffusion [50] and oxygen tracer diffusion [44, 51], exciding those for 3D perovskites. The literature data presented in Table 2 show that the values of the oxygen self-diffusion coefficient, D^*, for $La_2NiO_{4+\delta}$ measured using different techniques range from 10^{-8} to 10^{-10} $cm^2 \cdot s^{-1}$ at 700 °C. Moreover, $La_2NiO_{4+\delta}$ demonstrates a high value of the oxygen surface exchange constant, k^*, measured using SIMS analysis of the ^{18}O isotope as high as $2.16 \cdot 10^{-6}$ $cm^2 \cdot s^{-1}$ at 700 °C with E_k equal to 42 kJ · mol^{-1} [44].

However, it should be noted that oxygen migration in La_2NiO_4 is highly anisotropic [49, 54] with activation energies calculated for O^{2-} and O^- interstitial ions being equal to 0.88 and 0.29 eV for E_a (II ⊥ *a*, *b*) and 3.15 and 2.90 eV for E_a (⊥ *a*, *b*) (Figure 1). This fact was supported by the experimental isotopic exchange data on oxygen diffusion measured on single crystals [55], as well as by electrochemical measurements performed on the *a*-*b* plane oriented La_2NiO_4 [56].

Another important property that determines the possibility of using the material as an SOFC cathode is the coefficient of thermal expansion (CTE), as for correct operation and minimization of mechanical damage of the cell, CTEs of the electrode and electrolyte should be maximally close to each other. The thermal expansion coefficients (TEC) of $La_2NiO_{4+\delta}$ and traditionally used electrolytes are given in Table 3 (average in the temperature range of 50–900 °C).

From these data it can be concluded that $La_2NiO_{4+\delta}$ is thermo-mechanically compatible with ceria and $LaGaO_3$-based electrolytes, while it would be relevant to decrease the TEC value of $La_2NiO_{4+\delta}$ by appropriate doping to increase its compatibility with 8YSZ and apatite type electrolytes, as well as with some proton-conducting electrolytes (shown in Table 3).

Chemical compatibility of the electrode and electrolyte materials is no less important than the mechanical compatibility, especially under conditions of long-term operation at high temperatures. Excessive reactivity leads to the formation of insulating phases, decreasing ion transport, and increasing the polarization resistance at the cathode / electrolyte interface.

Several reactivity tests of $La_2NiO_{4+\delta}$ with both $Zr_{0.92}Y_{0.08}O_{2-y}$ and $Ce_{0.8}Gd_{0.2}O_{1.9}$ electrolytes performed by Montenegro-Hernández et al. [65] indicated the formation of secondary phases such as $La_{n+1}Ni_nO_{3n+1}$, $LaNiO_3$ and NiO. Besides, for the YSZ compound an insulating pyrochlore phase $La_2Zr_2O_7$ was obtained. Pikalova et al. also demonstrated higher reactivity $La_2NiO_{4+\delta}$ and $Ce_{0.8}Sm_{0.2}O_{1.9}$ compared to Ca-substituted one at high sintering temperature of the electrodes (> 1200 °C) [18]. Filippo et al. [66] carried out a comprehensive study of the reactivity between $La_2NiO_{4+\delta}$ and $Ce_{0.8}Gd_{0.2}O_{1.9}$, $La_9Sr_1Si_6O_{26.5}$ $La_{0.8}Sr_{0.2}Ga_{0.8}Mg_{0.2}O_{3-\delta}$, electrolytes. The powders were mixed in a mass ratio of

1 : 1 and annealed at 1150 °C for 1 h or at 800 °C for 5 days. Chemical compatibility study of $La_2NiO_{4+\delta}$ and $Ce_{0.8}Gd_{0.2}O_{1.9}$ after annealing at 800 °C for 5 days showed no interaction, whereas after annealing at 1150 °C for 1 h it was found that $La_2NiO_{4+\delta}$ completely decomposed into the higher order RP phase $La_4Ni_3O_{10}$. Similarly, prolonged annealing at 800 °C for 5 days of the $La_2NiO_{4+\delta}$ and $La_{0.8}Sr_{0.2}Ga_{0.8}Mg_{0.2}O_{3-\delta}$ mixture showed no significant interaction or decomposition, while after annealing at 1150 °C for 1 h, the presence of a small amount of lanthanum gallates ($LaSrGa_3O_7$ and $Sr_4Ga_2O_7$) and La_2O_3 was detected. These phases are known [67–69] to result from the slight decomposition of $La_{0.8}Sr_{0.2}Ga_{0.8}Mg_{0.2}O_{3-\delta}$ itself during sintering. Although the proportion of these impurities was small, their very low electrical conductivity and possible segregation at the electrode / electrolyte interface could negatively affect the operation of the fuel cell [66]. The interaction between $La_2NiO_{4+\delta}$ and $La_9Sr_1Si_6O_{26.5}$ was absent in both heating regimes studied. Antonova et al. [7] also observed no chemical interaction between $La_2NiO_{4+\delta}$ and an apatite-type $La_{10}(SiO_6)_4O_3$ electrolyte. Lyagaeva et al. [59] observed no significant chemical interaction $La_2NiO_{4+\delta}$ with $BaCe(Zr)_{0.8}Y_{0.2}O_{3-\delta}$ in 1 : 1 mixtures, calcined at 1100 °C for 10 h. No chemical interaction was found between $La_2NiO_{4+\delta}$ and the proton conducting $La_{0.9}Sr_{0.1}ScO_{3-\delta}$ electrolyte during heat treatment at 1100 °C for 3 h [21].

Ding et al. in [3] and Song et al. in [70] compared functionality of the $La_{n+1}Ni_nO_{3n+1}$ ($n = 1, 2, 3$) phases considered as cathode materials for SOFCs based on several physical and chemical properties, in particular, electrical conductivity. Figure 2a shows temperature dependences of the electrical conductivity of $La_2NiO_{4+\delta}$, $La_3Ni_2O_{7-\delta}$, and $La_4Ni_3O_{10-\delta}$, obtained in [70, 71]. As can be seen from the plot data, $La_2NiO_{4+\delta}$ has much lower conductivity values than the higher RP phases ($La_{n+1}Ni_nO_{3n+1}$, $n = 2, 3$). This phenomenon is explained by the fact that the complex oxide $La_2NiO_{4+\delta}$ has an electron-ionic type of conductivity, whereas the 2nd and 3rd order RP phases are predominantly electronic [70].

The study of the dependence of the electrical conductivity on the oxygen partial pressure carried out in [3, 70] showed that a decrease in the oxygen partial pressure leads to a decrease in the electrical conductivity (Figure 2b). It can be explained by the reversible loss of oxygen from the lattice and the reduction of Ni cations, the process being represented by Reactions (1, 2):

$$2Ni_{Ni}^{\bullet} + O_i'' \underset{pO_2\uparrow}{\overset{pO_2\downarrow}{\rightleftarrows}} 2Ni_{Ni}^{\times} + 0.5O_2 \qquad (1)$$

or

$$2h^{\bullet} + O_i'' \underset{pO_2\uparrow}{\overset{pO_2\downarrow}{\rightleftarrows}} 0.5O_2. \qquad (2)$$

This confirmed that the electron transfer in $La_2NiO_{4+\delta}$ is p-type [3, 15, 70, 72, 73, 74]. The temperature dependence of the electrical conductivity, observed for $La_2NiO_{4+\delta}$, e.g. in [42], has the extreme character of the curve view, the maximum on the curve is observed near 400 °C. The presence of a maximum on the temperature dependences of the electrical conductivity and its further decrease with increasing temperature were historically interpreted in different ways. Thus, the presence of a maximum on the temperature dependence of the conductivity was attributed to a semiconductor-metal phase transition [75] and a phase transition from the orthorhombic phase to the tetragonal phase [76]. Authors [3, 42, 77, 78] maintain the interpretation that the increase in electrical conductivity in the low temperature range is associated with an increase in the mobility

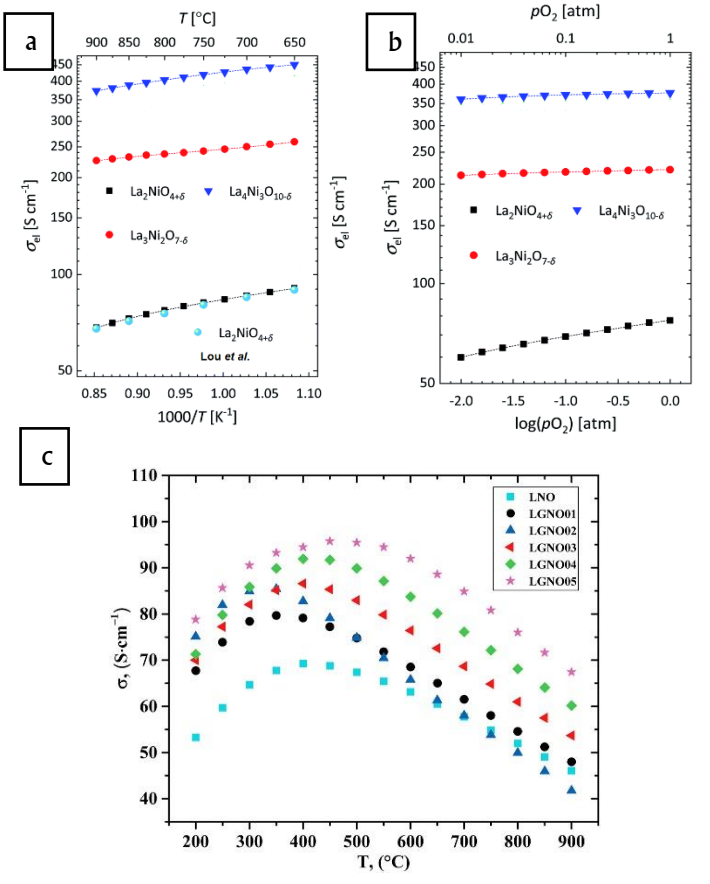

Figure 2 Temperature dependences of the electrical conductivity (a) and dependences of the electrical conductivity on oxygen partial pressure for $La_{n+1}Ni_nO_{3n+1}$ ($n = 1, 2, 3$) (b); temperature dependences of the electrical conductivity in $La_{2-x}Gd_xNiO_{4+\delta}$ ($x = 0.0$ denoted as LNO; $x = 0.1$–0.5 denoted as LGNO01–LGNO05, correspondingly) (c) ((a,b) are adopted from [70], Lou et al. [71]; (c) is reproduced from [42] with permission of Elsevier B.V.).

(number of jumps) of charge carriers – electron holes (or Ni^{3+} ions), and the appearance of the maximum and the decrease in electrical conductivity with increasing temperature in the range above 400 °C – with the release of excess interstitial oxygen from the sample, which results in a partial annihilation of the main charge carriers – electron holes due to the reduction of Ni^{3+} to Ni^{2+}. In addition, due to the larger radius of Ni^{2+} cations, this causes an increase in the Ni-O1 and Ni-O2 bond lengths, which, in the framework of the hopping mechanism, can additionally be a reason for decreasing the mobility of the electron holes.

This relationship was confirmed by the results of the thermogravimetric analysis provided, for example, in [42]. The end of the plateau on the TGA curves of δ-dependences on temperature, obtained upon heating in air, and the beginning of the decrease in the total oxygen content, or excess oxygen yield, coincided with the position of the maximum in the temperature dependence of the electrical conductivity. Based on the conclusions in [79], the characteristic behavior of the absolute oxygen content in $La_2NiO_{4+\delta}$ on heating could be influenced by two factors. The first is the presence of the phase transition of the nickelate from the orthorhombic to the tetragonal structure, which leads to an abrupt change in the binding energy of the interstitial oxygen ion with the lattice and therefore to a sharp change in the oxygen desorption rate. The second factor correlates with the unequal binding energy of oxygen atoms located at different crystallographic positions in the crystal lattice of the compounds. As the temperature increases, the separate successive removal of oxygen from the different positions proceeds in accordance with the increase in the binding energy of oxygen in the crystal lattice. It is therefore suggested that the end of the plateau at temperatures close to 400 °C (Figure 2c) corresponds to the release of over-stoichiometric oxygen from the interstitial sites of a nickelate crystal lattice, which is the weakest binding.

The presence of the mixed conductivity type in lanthanum nickelate $La_2NiO_{4+\delta}$ determines its high electrochemical properties. Gilev et al. [37] observed an increase in the polarization resistance, R_p, with increasing n in the $La_{n+1}Ni_nO_{3n+1}$ series as 0.75 (n = 1), 1.5 (n = 2), 2.25 (n = 3) $\Omega \cdot cm^2$ at 800 °C in air. Deep analysis of the impedance spectra using DRT technique allowed authors to define ionic transport in the electrodes as the slowest stage of the electrochemical reaction (middle frequency polarization resistance, R_{MF}). Despite facilitating oxygen exchange kinetics, an increase in the number of perovskite layers results in significant deterioration of ionic diffusion. Song et al. [70] demonstrated that the oxygen self-diffusion coefficients, D_s, calculated from the corresponding data on chemical diffusion oxygen non-stoichiometry, decrease profoundly with the order parameter n.

Based on the DRT analysis, Antonova et al. [19] proposed a physical model of the electrochemical process in the $La_2NiO_{4+\delta}$ electrode, identifying three main relaxation processes related to oxygen diffusion on the electrolyte / electrode interface (high-frequency process), charge transfer in the adsorption layer (medium-frequency process) and low-frequency process presented by Gerisher dispersion, attributed to oxygen surface exchange and diffusion in $La_2NiO_{4+\delta}$ and described by the parameters, which are consistent with the oxygen isotope exchange data [80]. A similar scheme for the $La_2NiO_{4+\delta}$ impedance fitting with the presence of the Gerisher element was proposed in [26].

Due to high electrochemical activity, $La_2NiO_{4+\delta}$ air electrodes were successfully used in both intermediate temperature SOFCs [17, 81, 82] and SOECs [83, 84], as well as reversible cells [85] with the performance significantly improved compared to the classical perovskite materials [86].

3. REE substituted $La_2NiO_{4+\delta}$

3.1. Correlation of the synthesis procedure and crystal structure

Solid solutions based on $La_2NiO_{4+\delta}$, obtained by substitution of lanthanum ions for rare earth ions, are currently considered as promising cathode materials for SOFCs, since their electrochemical activity can be improved compared to unsubstituted $La_2NiO_{4+\delta}$ due to increased oxygen content. So far, $La_{2-x}Ln_xNiO_{4+\delta}$ solid solutions have been studied, where the rare-earth element (Ln) has been chosen as an element substituting lanthanum in the A-position: Ln = Pr [34, 35, 45, 87–98]; Ln = Nd [34, 35, 43, 99–101]; Ln = Sm [34, 35, 102]; Ln = Eu [34, 35, 103]; Ln = Gd [34, 42, 72, 104]. In addition, it could be noted that some other series of Ruddlesden – Popper phases with the triple substitution on the La-site have been obtained recently, such as $La_{2-x-y}Nd_xPr_yNiO_{4+\delta}$ (x = 0.0; 0.3; 0.5 and y = 0.0; 0.2) in [43] and $La_{1.5-x}Eu_xPr_{0.5}Ni_{0.9}Cu_{0.1}O_{4+\delta}$ (x = 0.0; 0.1; 0.2; 0.3; 0.4; 0.6; 0.8) in [105].

Table 3 shows the properties (space groups and synthesis methods) of $La_{2-x}Ln_xNiO_{4+\delta}$ complex oxides. According to the literature data summarized in the table, the solid solutions obtained crystallized predominantly in the tetragonal syngony. The formation of an

orthorhombic crystal lattice was observed only in the case of dopant ions with a radius close to that of lanthanum ($La_{2-x}Ln_xNiO_{4+\delta}$ solid solutions, where Ln = Pr, Nd). As the radius of the dopant ion decreases, the tetragonal lattice stabilizes ($La_{2-x}Ln_xNiO_{4+\delta}$ solid solutions, where Ln = Sm, Eu, Gd). Note that for $La_{2-x}Ln_xNiO_{4+\delta}$ both types of crystal lattice can be realized depending on the amount of dopant and the synthesis method [34, 43]. According to the detailed crystallographic study performed by Vibhu et al. [87], in the $La_{2-x}Pr_xNiO_{4+\delta}$ series the compositions in the range of $0 < x < 0.5$ were single-phase and possessed a tetragonal structure (sp. gr. *I*4/*mmm*). Single-phase compositions with a monoclinic structure (sp. gr. *I*2/*m*) formed in the range of $1.0 < x \leq 2.0$. At the same time in the composition range of $0.5 \leq x \leq 1.0$ the authors observed coexistence of monoclinic and tetragonal phases.

The influence of thermal pre-treatment on the crystal structure of the $La_{2-x}Nd_xNiO_{4+\delta}$ compounds was investigated by Ishikawa et al. [99]. It was established that phases with a tetragonal structure formed at $x \leq 0.75$ for the quenched samples and at $x \leq 0.50$ for the annealed samples ($\delta \leq 0.15$), while the phases with an orthorhombic structure formed at $x > 0.75$ and at $x > 0.50$ ($\delta > 0.15$).

Table 4 – Crystal structure and synthesis techniques applied for $La_{2-x}Ln_xNiO_{4+\delta}$ (Ln = Pr, Nd, Sm, Eu, Gd).

Sample	Space group (structure)	Synthesis method, final annealing temperature, °C	Ref.
$La_{2-x}Pr_xNiO_{4+\delta}$ $x = 0.0, 0.6$	*Fmmm (O)*	Solid-state route, 1350	[93]
$x = 1.0, 1.4, 2.0$	*Bmab (O)*		
$x = 0.0, 0.5, 1.0$	*Fmmm (O)*	Electrostatic atomization method, 950	[45]
$La_{1.7}Nd_{0.3}NiO_{4+\delta}$	*Fmmm (O)*	Citrate-nitrate combustion, 1000	[16]
$La_{1.6}Nd_{0.4}NiO_{4+\delta}$	*I*4/*mmm (T)*	Glycerol-nitrate combustion, 1200	[34], [35]
$La_{2-x}Sm_xNiO_{4+\delta}$ $0.0 \leq x \leq 1.1$, $\Delta x = 0.1$	*I*4/*mmm (T)*	Pechini method, 800	[102]
$La_{1.6}Sm_{0.4}NiO_{4+\delta}$	*I*4/*mmm (T)*	Glycerol-nitrate combustion, 1200	[34]
$La_{2-x}Eu_xNiO_{4+\delta}$ $x = 0.0, 0.2, 0.4, 0.6, 0.8$	*I*4/*mmm (T)*	Solid-state route, 1250	[103]
$La_{2-x}Gd_xNiO_{4+\delta}$ $x = 0.0, 0.1, 0.2, 0.3, 0.4, 0.5$	*I*4/*mmm (T)*	Formate pyrolysis, 1350	[42]
$La_{2-x}Gd_xNiO_{4+\delta}$ $x = 0.0, 0.2, 0.4$	*I*4/*mmm (T)*	Glycerol-nitrate combustion, 1200	[72]

Pikalova et al. [34] studied the change in unit cell parameters and volume for $La_{1.6}Ln_{0.4}NiO_{4+\delta}$ (Ln = Pr, Nd, Sm, Eu, Gd) as a function of the ionic radius of the dopant in the A-position (Figure 3a). The observed decrease in the cell parameters and volume with decreasing the dopant radius was in strong accordance with the Vegard's law [106].

Based on the structural data represented in literature, Guseva et al. [107] analyzed the concentration dependences of the parameters and volume of $La_{2-x}Ln_xNiO_{4+\delta}$ complex oxides. It is shown that for all series the parameters *c* and *V* have a linear dependence, both on the composition of the solid solution, and on the average radius (r_{avg}) of the ion in the A-site (Figure 3a and 3b). By approximating the experimental points, the equations of the planes $c = f(x, r_{avg})$ and $V = f(x, r_{avg})$ were determined, which make it possible to predict the parameter values and the structure of complex solid solutions.

It is also shown that the course of the concentration dependences of *a* and *b* parameters on the average radius of the A-site ion is more complex (Figure 4a and 4b). This is due to the fact that due to the introduction of interstitial oxygen into the rock salt layers in order to increase the

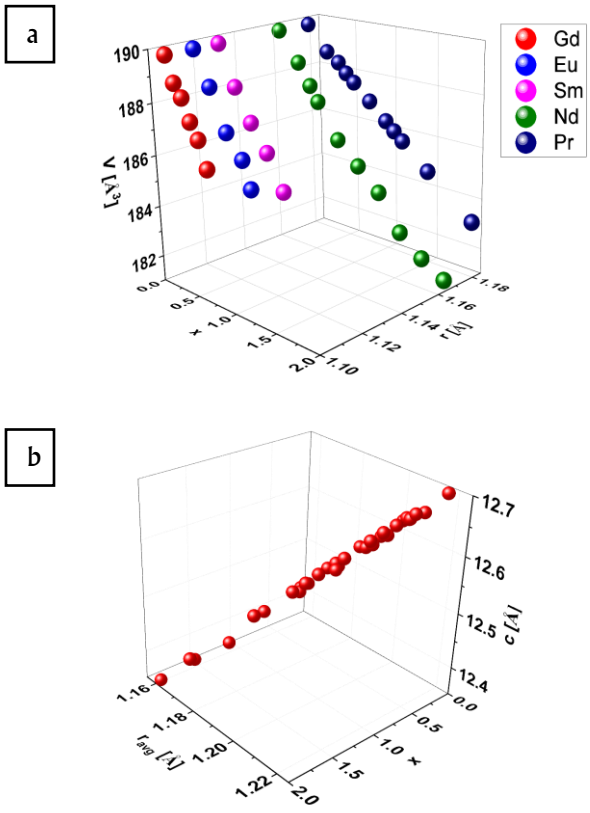

Figure 3 Dependences obtained for $La_{2-x}Ln_xNiO_{4+\delta}$ on the content and ionic radius of the Ln^{3+} dopant: unit cell volume, *V* (a); *c* lattice parameter (b) (Ln = Pr [34, 87], Nd [34, 99, 100], Eu [34, 103], Sm [107], Gd [42].

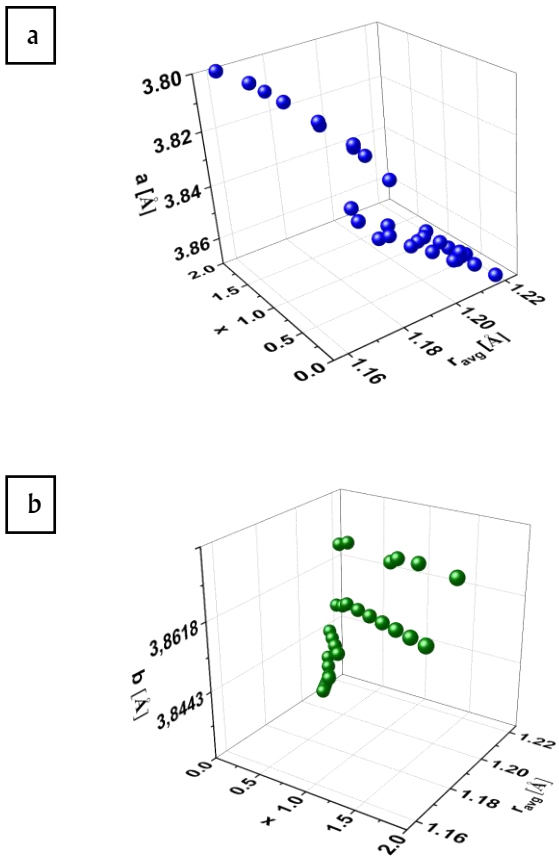

Figure 4 Dependences obtained for $La_{2-x}Ln_xNiO_{4+\delta}$ on the content and ionic radius of the $Ln^{3+}{}_{IX}$ dopant: *a* lattice parameter (a); *b* lattice parameter (b) (Ln = Pr [34, 87], Nd [34, 99, 100], Eu [34, 103], Sm [107], Gd [42].

stability of the RP phase, the data values parameters are determined not only by the composition x and the size of the A-site ion, but also depend on the value of oxygen non-stoichiometry, i.e. $a = f(x, r_{avg}, \delta)$, $b = f(x, r_{avg}, \delta)$.

These data prove that stabilization of the original structure of a Ruddlesden – Popper phase, having the size discrepancy of the perovskite La(Ln)NiO_3 and the rock-salt layers La(Ln)O in the *a, b*-plane [108] upon lanthanum substitution in the A-position is due to the intercalation of the excess interstitial oxygen into the oxide lattice. The increase in over-stoichiometric oxygen leads to a change in the degree of oxidation of nickel from Ni^{+2} to Ni^{+3}, which has a smaller radius (according to [109], the ionic radii of $Ni^{3+}{}_{VI}$ are equal to 0.56 Å for the low-spin state and 0.60 Å for the high-spin state compared to the ionic radius of $Ni^{2+}{}_{VI}$, which is equal to 0.69 Å). Table 5 summarizes the values of the tolerance factors calculated without and with considering the excess interstitial oxygen and absolute oxygen non-stoichiometry for $La_{1.6}Ln_{0.4}NiO_{4+\delta}$ solid solutions [34]. As it can be seen from Table 5, the Goldschmidt tolerance factor *t*, which is

Table 5 – Values of tolerance factors and absolute oxygen non-stoichiometry of complex oxides $La_{1.6}Ln_{0.4}NiO_{4+\delta}$ depending on the Ln substituent element [34]

Value	Ln = Pr	Ln = Nd	Ln = Sm	Ln = Eu	Ln = Gd
t^a	0.882	0.881	0.879	0.879	0.878
δ	0.18(1)	0.17(1)	0.17(1)	0.16(1)	0.14(1)
$t_{ox}{}^b$	0.896	0.895	0.892	0.891	0.888

[a] – calculated without δ account;
[b] – calculated with δ account.

a quantitative assessment of the presence of microstrains in the crystal lattice [110, 111], increases significantly when oxygen is incorporated into the oxide lattice, thus demonstrating the stabilization of the phase by increasing the value of the oxygen non-stoichiometry.

3.2. Oxygen transport properties

There are a limited number of the studies on oxygen diffusion In REE substituted $La_2NiO_{4+\delta}$. Vibhu et al. [44, 112] reported D^* values for the substituted samples in the $La_{2-x}Pr_xNiO_{4+\delta}$ series to be in the range of those reported for $La_2NiO_{4+\delta}$ and $Pr_2NiO_{4+\delta}$ ($1.5 \cdot 10^{-8}$–$2.5 \cdot 10^{-8}$ $cm^2 \cdot s^{-1}$ at 600 °C). The authors noted that k^* values were slightly higher than those for the base materials. Usenka et al. [95] investigated temperature programmed oxygen desorption-sorption (TPD) processes in $Pr_{2-x}La_xNiO_{4+\delta}$ compositions. The TPD spectra of the doped samples were found to exhibit two sharp peaks related to the removal of oxygen from different sites of the crystal lattice. When increasing the Pr amount, the oxygen desorption shifted to lower temperature compared to $La_2NiO_{4+\delta}$. The TPD spectrum of $Pr_2NiO_{4+\delta}$ recorded under the same conditions exhibited three sharp and two local maxima in the range of the temperature of 210–700 °C and prominent maximum fourth above 600 °C. These maxima were supposed to relate to 1) removal of interstitial sites with the coordinates (¼, ¼, ¼) (around 200 °C); 2) orthorhombic-tetragonal phase transition (370 °C); 3) (non-equilibrium) migration positions of mobile oxygen from the crystal lattice under heating (400–650 °C); and 4) removal of oxygen from NiO_6 octahedra of the perovskite layers above 650 °C). It was shown that removal of oxygen from the perovskite layers occurred at δ equal to 0.07–0.09 for $Pr_{2-x}La_xNiO_{4+\delta}$ and δ equal to 0.12–0.14 for $Pr_2NiO_{4+\delta}$.

Sadykov et al. [104] investigated oxide ionic transport features in $La_{2-x}Gd_xNiO_{4+\delta}$ (x = 0.0–0.4) using the mass relaxation method and oxygen isotope exchange with $C^{18}O_2$ in a flow reactor. Both techniques demonstrated a decrease in oxygen mobility and surface reactivity with doping. Substitution Gd for La resulted in the emergence of oxygen diffusivity nonuniformity. The authors

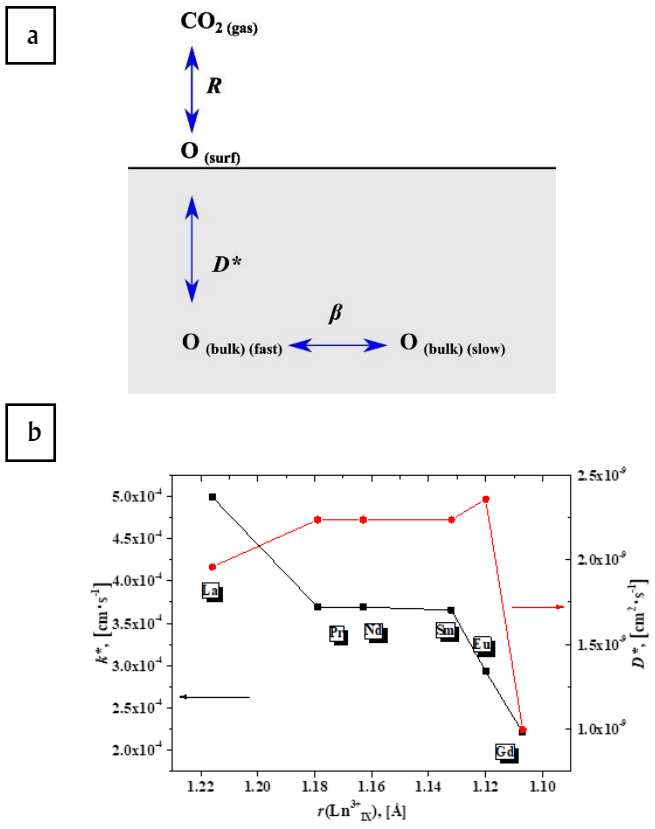

Figure 5 Schematic illustration for the mathematical model of oxygen isotope exchange with $C^{18}O_2$ in the flow reactor for Gd-doped $La_2NiO_{4+\delta}$ (a); comparison of oxygen surface exchange constant (k^*) and tracer diffusion coefficient (D^*) at 700 °C for the $La_{1.6}Ln_{0.4}NiO_{4+\delta}$ samples (b) ((a) is reproduced from [104] with permission of Elsevier B.V.; (b) is reproduced from [34] with permission of Elsevier B.V.).

proposed a mathematical model with a fast diffusion channel (via cooperative mechanism of oxygen migration) and a slower exchange with the neighboring oxide anions for the description of oxygen transport in $La_{2-x}Gd_xNiO_{4+\delta}$ (Figure 5a).

This model was further applied for the fitting of the isotope exchange data obtained by authors for the $La_{1.6}Ln_{0.4}NiO_{4+\delta}$ series (Ln = Pr, Nd, Sm, Eu, Gd) [34]. The authors noted that all substituted samples were characterized as having fast oxygen diffusivity provided by a cooperative mechanism of oxygen migration involving both regular and highly mobile interstitial oxygen. However, the contribution of fast oxygen to the overall exchange decreased with doping as 92 % for undoped LNO, 90 % for Gd-doped, 87 % for Pr, Sm, Nd-doped, and 83 % for Eu-doped. Comparison of the oxygen exchange parameters obtained for the samples with different dopants (Figure 5b) revealed that both the oxygen tracer diffusion coefficient and the surface exchange constant tend to slightly increase and then decrease in the row with a broad maximum observed for Pr, Nd, and Sm-doped samples, while the effective activation energy characterizing the oxygen migration barrier did not vary within the calculation error in the series. The authors argue that this fact implies that oxygen diffusion characteristics vary not due to the migration barrier value, but mainly due to the mobile oxygen content.

3.3. Functional properties

Table 6 summarizes the data on the values of the thermal expansion coefficients for $La_{2-x}Ln_xNiO_{4+\delta}$ (Ln = Pr, Nd, Sm, Eu, Gd) complex oxides obtained in air in the temperature range from 50 °C (T_l) to 900 °C (T_h), if not shown specifically.

T_c usually correlates with the beginning of oxygen release from the layered structure of the oxide and is individual for every specific dopant. Thus, difference in TECs below and above T_c occurs presumably due to chemical expansion [114] associated with the loss of interstitial oxygen from the crystal structure which is compensated by the corresponding reduction in the Ni^{3+}/Ni^{2+} ratio. This results in compressive stress in the oxide structure along the *c* axis and tensile stresses in the *a, b* layers. Due to these processes compensating each other, all La_2NiO_4-based derivatives demonstrate significantly lower chemical expansion than most perovskite materials. Comparing Table 3 and 5 it can be

Table 6 – TEC values for REE or AEE substituted $La_2NiO_{4+\delta}$.

Composition	TEC · 10⁶, K⁻¹			Ref.
	$T_l < T_c$	$T_h > T_c$	$T_l - T_h$	
$La_{1.9}Gd_{0.1}NiO_{4+\delta}$	12.3	12.3	12.3	[42]
$La_{1.8}Gd_{0.2}NiO_{4+\delta}$	12.2	13.6	13.6	
$La_{1.7}Gd_{0.3}NiO_{4+\delta}$	12.2	12.5	12.5	
$La_{1.6}Gd_{0.4}NiO_{4+\delta}$	12.4	12.4	12.4	
$La_{1.5}Gd_{0.5}NiO_{4+\delta}$	11.9	13.5	13.5	
$La_{1.8}Sm_{0.2}NiO_{4+\delta}$	12.56	12.77	12.68	[113]
$La_{1.6}Sm_{0.4}NiO_{4+\delta}$	12.81	12.89	12.82	
$La_{1.4}Sm_{0.6}NiO_{4+\delta}$	12.24	12.27	12.28	
$La_{1.6}Pr_{0.4}NiO_{4+\delta}$	14.1	15.2	[a]14.6	[35]
$La_{1.6}Nd_{0.4}NiO_{4+\delta}$	13.8	15.1	14.5	
$La_{1.6}Eu_{0.4}NiO_{4+\delta}$	13.6	15.3	14.4	
$La_{1.6}Sm_{0.4}NiO_{4+\delta}$	13.5	15.0	14.2	
$La_{1.5}Pr_{0.5}NiO_4$			[b]15.0	[92]
La_2NiO_4			[c]13.1	[58]
$La_{1.6}Sr_{0.4}NiO_{4+\delta}$			13.6	
$La_{1.2}Sr_{0.8}NiO_{4+\delta}$			12.8	
$La_{1.7}Ca_{0.3}NiO_4$			[d]13.9	[63]
$La_{1.7}Sr_{0.3}NiO_4$			14.2	
$La_{1.7}Ba_{0.3}NiO_4$			15.2	

[a] – 200–1000 °C;
[b] – 50–1000 °C;
[c] – 30–1000 °C;
[d] – 100–900 °C.

concluded that substitution with Gd, Sm and Ca results in decreasing TEC values. Moreover, these derivatives are chemically more compatible with CeO_2-based electrolytes compared to undoped $La_2NiO_{4+\delta}$ [18, 42, 113].

According to [72, 92, 93, 113], REE substitution of lanthanum in $La_2NiO_{4+\delta}$ resulted in an increase in electrical conductivity. This was explained by the fact that the observed decrease in unit cell parameters (and bond lengths) led to an increase in carrier mobility via the small radius polaron mechanism, as it was observed earlier for the RP phases in [115, 116]. At low concentration of the dopant ($x \leq 0.4$), REE substitution may have an even more pronounced influence on the conductivity of the base oxide compared to some AEE, introducing additional defects due to charge compensation (Figure 6a).

However, at a high substitution level, increasing the conductivity in the REE-substituted $La_2NiO_{4+\delta}$ series becomes less and less pronounced. As for example, for the $La_{2-x}Pr_xNiO_{4+\delta}$ series in the range of $0 \leq x \leq 1$ an increase in Pr content resulted in increasing the conductivity (from 50 to 110 $S \cdot cm^{-1}$), while there was almost no difference between the conductivity of the doped composition at

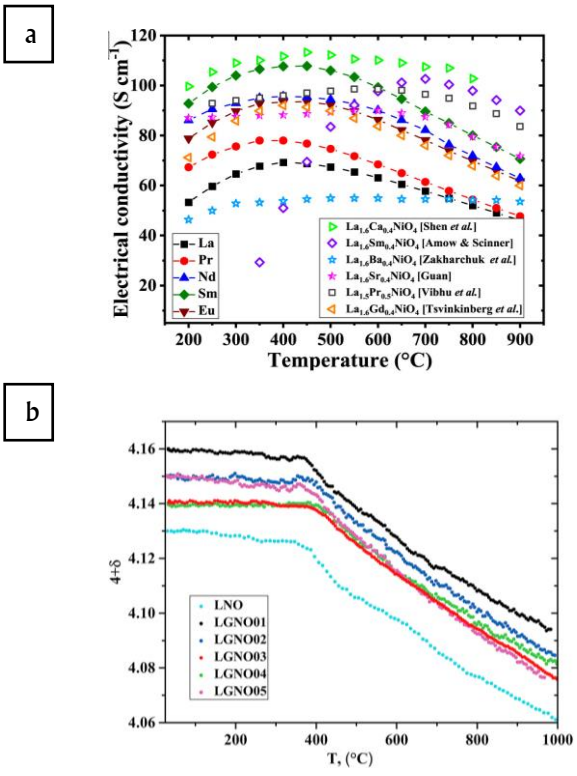

Figure 6 Temperature dependences of electrical conductivity for $La_{1.6}Ln_{0.4}NiO_{4+\delta}$, where Ln = La, Pr, Nd, Sm, Eu, compared with data of Shen et al. [117], Amow & Skinner [102], Zakharchuk et al. [118], Guan [119], Vibhu et al. [98], Tsvinkinberg et al. [42] for doped $La_2NiO_{4+\delta}$ (a); temperature dependences of the absolute oxygen content for $La_{1.6}Ln_{0.4}NiO_{4+\delta}$, where Ln = La, Pr, Nd, Sm, Eu (b) ((a, b) are reproduced from [35] with permission of Elsevier B.V.).

$x = 1.0$ and 2.0 [112]. Similar tendency was found for Gd and Sm doped systems, where conductivity reached "saturation" at $x = 0.4$–0.5 (90–96 $S \cdot cm^{-1}$ at 450 °C and $x = 0.6$–0.8 (111–112 $S \cdot cm^{-1}$), respectively. Significantly higher values of total conductivity can be achieved at high doping levels in the $La_{2-x}Sr_xNiO_{4+\delta}$ (273 $S \cdot cm^{-1}$ at 600 °C, $x = 0.75$ [120]) and in the $La_{2-x}Ba_xNiO_{4+\delta}$ series (127 $S \cdot cm^{-1}$ at 600 °C, $x = 0.5$) [118]. However, despite higher total conductivity values, the ionic component of conductivity in such materials drops significantly with doping, which may result in deterioration of electrochemical properties of the related electrodes [46].

It should be noted that, in contrast to the character of the electrical conductivity curve for AEE substituted $La_2NiO_{4+\delta}$, temperature dependences of conductivity for $La_{2-x}Ln_xNiO_{4+\delta}$ also exhibit extremal behavior. As in the case of $La_2NiO_{4+\delta}$, the peak value of the electrical conductivity for $La_{2-x}Ln_xNiO_{4+\delta}$ (Ln = Pr, Nd, Sm, Eu, Gd) correlates with the beginning of the oxygen release, which is responsible for the sharp decrease at the thermogravimetric curves after the horizontal plateau, as seen from (Figure 6b).

3.4. Electrochemical performance

The electrochemical activity of $La_2NiO_{4+\delta}$-based materials is traditionally studied using impedance spectroscopy. There are several ways of presenting impedance data, the most common being Nyquist plots and relaxation time distributions. The relaxation time distribution method uses a Fourier transform to provide a greater degree of separation between processes. The shape of the peak reflects the nature of the process occurring in the system, so the resulting plot gives an indication of the number and magnitude of the processes occurring. The information obtained can be used to select elements in the equivalent circuit method. The electrochemical properties of $La_2NiO_{4+\delta}$ have been studied using impedance spectroscopy by the equivalent circuit method with analysis of the distribution of relaxation times [19, 81, 121–125]. The authors consider that the oxygen reduction process at the cathode, $La_2NiO_{4+\delta}$, consists of three stages. In [122] three contributions to the process are described in detail:

- High frequency process – the resistance of this contribution decreases with increasing the temperature and does not depend on the partial pressure of oxygen; it can be caused by the transfer of oxygen ions across the electrolyte / electrode interface. The ohmic capacitance of the process was $5 \cdot 10^{-7}$ $F \cdot cm^{-2}$ and the relaxation frequency was 10^5 Hz.
- Medium frequency process – the contribution of

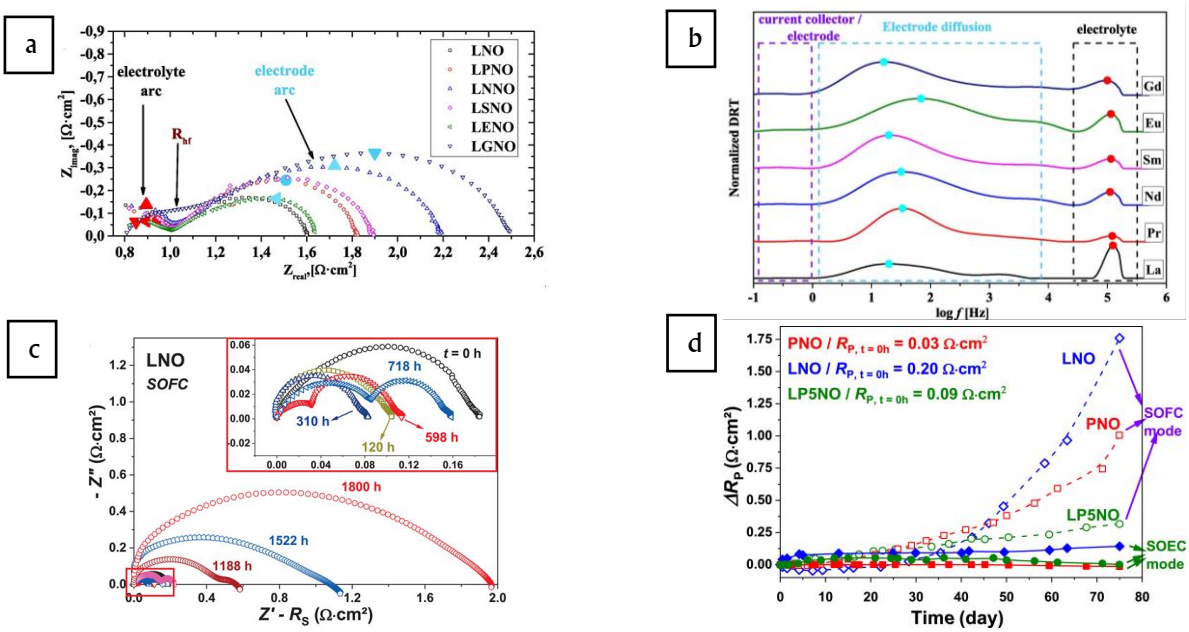

Figure 7 Impedance spectra for the $La_{1.6}Ln_{0.4}NiO_{4+\delta}$ electrodes sintered at 1200 °C with the $LaNi_{0.6}Fe_{0.4}O_{3-\delta}$ + CuO collector layer ($La_2NiO_{4+\delta}$ denoted as LNO, $La_{1.6}Pr_{0.4}NiO_{4+\delta}$ as LPNO, $La_{1.6}Nd_{0.4}NiO_{4+\delta}$ as LNNO, $La_{1.6}Sm_{0.4}NiO_{4+\delta}$ as LSNO, $La_{1.6}Eu_{0.4}NiO_{4+\delta}$ as LENO, $La_{1.6}Gd_{0.4}NiO_{4+\delta}$ as LGNO) (a); DRT analysis of the spectra for the $La_{1.6}Ln_{0.4}NiO_{4+\delta}$ (Ln = La, Pr, Nd, Sm, Eu, Gd) electrodes collected at 700 °C in air (b); Nyquist plots for $La_2NiO_{4+\delta}$ aged at 700 °C for 1800 h at i_{dc} = 300 mA · cm^{-2} in the SOFC mode (c); Time plots of polarization difference ΔRP for $La_{2-x}Pr_xNiO_{4+\delta}$ ($La_2NiO_{4+\delta}$ denoted as LNO, as LP5NO, $Pr_2NiO_{4+\delta}$ as PNO), aged at 700 °C for 1800 h at i_{dc} = 300 mA · cm^{-2} in the SOFC and SOEC modes (d) ((a, b) are reproduced from [34] with permission of Elsevier B.V.; (c, d) are reproduced from [90]).

this resistance decreases with increasing the temperature and the oxygen partial pressure. The process may be related to the diffusion of oxygen atoms with subsequent charge transfer, the capacitance and relaxation frequency were 10^{-4} F · cm^{-2} and 10^3 Hz respectively.

• Low frequency process – the resistance of this contribution decreases with increasing temperature and becomes dominant at low partial pressures. The capacitance of the process was 10^{-1} F · cm^{-2}, and the relaxation frequency was 1 Hz. The process can be related to the phenomenon of molecular oxygen dissociation; the same view is taken in [126].

The total resistivity of the oxygen reduction process was obtained by summing the individual resistances associated with each stage. It decreases significantly with increasing temperature and insignificantly with increasing oxygen partial pressure [122].

The group led by Pikalova has extensively investigated the electrochemical activity of the Ln-substituted $La_2NiO_{4+\delta}$: $La_{2-x}Gd_xNiO_{4+\delta}$ in [10, 72] and $La_{1.6}Ln_{0.4}NiO_{4+\delta}$ (Ln = Pr, Nd, Sm, Eu) in [34, 35]. Figures 7a and 7b show typical impedance spectra for the $La_{1.6}Ln_{0.4}NiO_{4+\delta}$ (for Ln = La, Pr, Nd, Sm, Eu, Gd samples were designated as LNO, LPNO, LNNO, LSNO, LENO, LGNO, respectively) electrodes, sintered at 1200 °C, with the $LaNi_{0.6}Fe_{0.4}O_{3-\delta}$ + 3 wt. % CuO collector layer (CL), sintered at 900 °C, which were collected at 700 °C in air, and DRT analysis of the above spectra, respectively. According to the DRT analysis performed by the authors, processes with an equivalent capacity of ~10^{-6}–10^{-7} F · cm^{-2} (the area highlighted in black in Figure 7b) are associated with the ohmic electrolyte resistance. A process with a capacity of ~10^{1} F · cm^{-2} (highlighted in violet in Figure 7b) the authors considered as describing the electron transfer at the current collector / electrode interface. Due to high conductivity of the collector layer, the contribution of this process was less significant compared to other processes. In the medium-frequency range, the presence of the Gerisher dispersion (the area highlighted in blue in Figure 7b) is clearly seen, which is mathematically equivalent to the dispersion given in the Adler – Lane – Steel (ALS) model [127, 128] to describe the electrochemical behavior of MIEC electrodes:

$$Z_{chem} = R_{chem}\frac{1}{\sqrt{1+j\omega\tau_{chem}}}, \quad (3)$$

where Z_{chem}, R_{chem} and τ_{chem} are the impedance diffusion part related to non-charge-transfer processes, resistance, and time constant, respectively. Using this equivalency, the authors established a close correlation of electrode performance with oxygen transport properties of the related MIEC electrode materials using the following equation [129]:

$$R_{chem} = \frac{RT}{4F^2}\sqrt{\frac{\tau}{(1-\varepsilon)4ac_O x_\delta^O D^* k^*}}, \quad (4)$$

where R, F are the universal gas and Faraday constants; ε, τ are electrode porosity and tortuosity, defined by the authors from the electron images of the electrode microstructure; a is specific surface area of electrode powders, c_O, x_δ^O are concentration of oxygen lattice sites involved in the diffusion mechanism and molar fraction of O-defects at equilibrium; k^*, D^* are oxygen surface exchange constant and tracer diffusion coefficient, respectively. The values for the diffusion impedance, R_{chem}, were calculated by the authors using the impedance spectroscopy data and amounted 0.59 Ω · cm² for LNO, 0.63 Ω · cm² for LENO, 0.79 Ω · cm² for LPNO, 0.87 Ω · cm² for LSNO, 1.14 Ω · cm² for LNNO, and 1.52 Ω · cm² for LGNO, respectively. The values of r_O, D^*, k^*, calculated in the framework of the Adler – Lane – Steele (ALS) model using the impedance spectroscopy data, were shown to be in a good agreement with the data obtained by the temperature-programmed isotope exchange of oxygen with $C^{18}O_2$ in a flow reactor using materials of the $La_{1.6}Ln_{0.4}NiO_{4+\delta}$ series. The data, obtained in [34, 35], for the two-layer electrodes with functional $La_{1.6}Ln_{0.4}NiO_{4+\delta}$ layers in comparison with results for $La_{2-x}Ln_xNiO_{4+\delta}$ from the other works are summarized in Table 7. As can be seen from the data in the Table, the smallest value of the polarization resistance, equal to 0.184 Ω · cm² at 700 °C, was measured by Zhao et al. in [92] for the $La_{1.5}Pr_{0.5}NiO_{4+\delta}$ electrode. Summarizing the data in Table 7, it is worth noting that R_p values depend on both the composition of the solid solution and the composition of the electrolyte.

It is important to note that the method of synthesis of the complex oxide affects its electrochemical properties. For example, $La_{1.6}Eu_{0.4}NiO_{4+\delta}$ obtained by the solid phase method and by combustion of glycerol nitrate compositions had values of R_p = 1.6 [103] and 0.63 Ω · cm², respectively, at 700 °C [34]. In addition, according to the study [35] the sintering temperature and collector layer (CL) using both influence on the electrode activity. For $La_{1.6}Eu_{0.4}NiO_{4+\delta}$ with CL, sintered at 1100 and 1200 °C, R_p values were equal to 3.35 and 0.64 Ω · cm², respectively, at 700 °C, although for $La_{1.6}Eu_{0.4}NiO_{4+\delta}$ with and without CL, sintered at 1200 °C, R_p values were equal to 0.64 and 0.70 Ω · cm², respectively, at 700 °C [35].

The electrochemical activity of the $La_{2-x}Pr_xNiO_{4+\delta}$ based (x = 0.0; 0.5; 2.0) cells during long-term operation was investigated in [90]. Symmetric cells for polarization impedance measurements were fabricated by applying a cathode slurry to the electrolyte by screen printing. Yttrium stabilized zirconia (YSZ) was chosen as the electrolyte. Figure 7c shows the normalized impedance spectra of a $La_2NiO_{4+\delta}$ sample aged at 700 °C for up to 1800 h at a constant current i_{dc} = 300 mA · cm⁻² in the fuel cell (SOFC) operating mode. It was found that the polarization resistance increased from R_p = 0.18 Ω · cm² to 2 Ω · cm² after 1800 h (+ 1110 %) [90].

To facilitate the analysis of the variation of the electrochemical activity of the cell with time, a polarization difference dependence graph was plotted (Figure 7d) $\Delta R_P = R_{Pgt} - R_{Pini}$, where R_{Pini} and R_{Pgt} are the polarization resistances at t = 0 h and at the given time, respectively. The data obtained showed that in the fuel cell mode, $La_{1.5}Pr_{0.5}NiO_{4+\delta}$ is characterized by a decrease in

Table 7 – The polarization resistance values for $La_{2-x}Ln_xNiO_{4+\delta}$ - based electrodes at 700 °C.

Cathode	R_p, Ω · cm²	Electrolyte	Ref.
$La_2NiO_{4+\delta}$	0.57	$Ce_{0.8}Sm_{0.2}O_{1.9}$	[26]
$La_2NiO_{4+\delta}$	0.85	$Ce_{0.8}Sm_{0.2}O_{1.9}$	[35]
$La_{1.6}Pr_{0.4}NiO_{4+\delta}$	0.82		
$La_{1.6}Nd_{0.4}NiO_{4+\delta}$	1.18		
$La_{1.6}Sm_{0.4}NiO_{4+\delta}$	0.89		
$La_{1.6}Eu_{0.4}NiO_{4+\delta}$	0.64		
$La_{1.9}Sm_{0.1}NiO_{4+\delta}$	11	$La_{0.8}Sr_{0.2}Ga_{0.8}Mg_{0.2}O_{3-\delta}$	[102]
$La_{0.9}Sm_{1.1}NiO_{4+\delta}$	18		
$La_2NiO_{4+\delta}$	2.8	$Ce_{0.8}Sm_{0.2}O_{1.9}$	[103]
$La_{1.8}Eu_{0.2}NiO_{4+\delta}$	1.3		
$La_{1.6}Eu_{0.4}NiO_{4+\delta}$	1.6		
$La_{1.4}Eu_{0.6}NiO_{4+\delta}$	4.6		
$La_{1.2}Eu_{0.8}NiO_{4+\delta}$	2.6		
$La_2NiO_{4+\delta}$	0.78	$Ce_{0.8}Gd_{0.2}O_{1.9}$	[72]
$La_{1.8}Gd_{0.2}NiO_{4+\delta}$	0.92		
$La_{1.6}Gd_{0.4}NiO_{4+\delta}$	1.9		
$La_{1.5}Pr_{0.5}NiO_{4+\delta}$	0.18	$Ce_{0.8}Sm_{0.2}O_{1.9}$	[92]

polarization resistance compared to the non-substituent $La_2NiO_{4+\delta}$ sample [90].

So, the results of physicochemical property and electrochemical activity studies for $La_{2-x}Ln_xNiO_{4+\delta}$ (Ln = Pr, Nd, Sm, Eu) [34, 35], $La_{2-x}Pr_xNiO_{4+\delta}$ [43, 45, 90–93, 96, 98, 130] and $La_{2-x}Gd_xNiO_{4+\delta}$ [34, 42, 72, 104] show that, firstly, optimal doping of basic lanthanum nickelate $La_2NiO_{4+\delta}$ with REE ions can improve physicochemical properties such as electrical conductivity, polarization resistance and mechano-thermal compatibility with traditionally used electrolytes in SOFCs. Secondly, a study by Pikalova et al. [35] showed that it is the doping of lanthanum nickelate $La_2NiO_{4+\delta}$ with Sm that gives better electrical conductivity results compared to other rare earth elements such as Pr, Gd [42, 98, 102].

4. Conclusions and future perspectives

The literature review allows us to conclude that doping lanthanum nickelate $La_2NiO_{4+\delta}$ with rare-earth element ions can improve the functional properties of this oxide material from the point of view of its use as a cathode for intermediate-temperature SOFCs. First, the REE doping does not lead to the formation of carbonates on the surface of the working cathode, which is typical of $La_2NiO_{4+\delta}$ materials doped with alkaline earth elements. Second, this kind of doping allows preservation or even rising the interstitial oxygen content, thus improving electrode oxygen transport properties and, as a result, the electrode performance. It should be noted that among the solid solutions of general composition $La_{2-x}Ln_xNiO_{4+\delta}$ (Ln = Pr, Nd, Sm, Eu, Gd) studied so far, those of $La_{2-x}Sm_xNiO_{4+\delta}$ are the least studied: there are very few studies in the literature for a wide range of compositions on the analysis of a crystal structure, thermomechanical and chemical compatibility with electrolyte materials intermediate-temperature SOFCs, electrical conductivity, polarization resistance. Due to the relevance of the studies on the doping of $La_2NiO_{4+\delta}$ with REE ions and the limited literature data for Ln = Sm, as well as for combinations of two or more REE dopants, the future works could be directed on these complex oxide systems starting from their physicochemical properties and further to possible application in SOFC and SOEC cells.

Supplementary materials

No supplementary materials are available.

Funding

This research had no external funding.

Acknowledgments

The authors are grateful to Mr. Roman Ivanov, engineer of the Department of Technical Physics, Physico-technological Institute UrFU, for help with the graphical visualization of data.

Author contributions

Elena Pikalova: Conceptualization; Visualization; Project administration; Writing – Review & Editing.

Ekaterina Guseva: Methodology; Visualization; Writing – Original draft; Investigation; Data curation.

Elena Filonova: Software; Validation; Supervision; Writing – Original draft; Writing – Review & Editing.

Conflict of interest

The authors declare no conflict of interest.

Additional information

Elena Pikalova, Ph. D, senior researcher of the Laboratory of Kinetics, IHTE UB RAS (Yekaterinburg, Russia), the leader of the group on the development of cathode materials for SOFCs and the head researcher in the group of Engineering and economic interdisciplinary research in energy and high-tech industries at the Department of Environmental Economics, Graduate School of Economics and Management, Ural Federal University. She is the author of 114 research papers, h-index 26 (WoS ResearcherID: L-6877-2017; Scopus Author ID: 16242376500; ORCID: 0000-0001-8176-9417), 10 patents and one monograph. Area of scientific interests and research: alternative energy sources, SOFCs, solid state electrolytes, thin-film technologies, cathode materials, MIEC membranes, impedance spectroscopy.

Guseva Ekaterina, laboratory assistant-researcher of the Department of Chemical Materials Science, UrFU (Yekaterinburg, Russia). Now, she is studying for a master's degree in "Chemistry" at the Department of Fundamental and Applied Chemistry, Ural

Federal University, ORCID: 0009-0009-5940-6228. She twice became a laureate of youth scientific conferences. Since 2023, she has been the executor of the RNF grant. Area of scientific interests and research: cathode materials, high-entropy oxides (HEOs), solid oxide fuel cells (SOFCs).

Elena Filonova, Ph. D., Associate Professor at the Department of Physical and Inorganic Chemistry, is Leading Lecturer of "Statistical Thermodynamics" at the Department of Chemistry and "Information Sources in Chemistry" at the School of Sciences, Institute of Natural Sciences and Mathematics, Ural Federal University (Ekaterinburg, Russia). International Expert-consultant on information sources Elsevier. Author of 70 documents indexed in Scopus database with h-index 17 (Scopus Author ID: 6602857032, WoS ResearcherID: K-9536-2017, ORCID: 0000-0002-7273-7525). Fields of scientific interest and research: Chemical Thermodynamics, Scientometrics. Research interests include development of synthesis techniques, characterization of materials and investigation of their functional properties for SOFC and catalysis applications. Specialist in refinement crystal structure of materials using the Rietveld method.

References

1. Nirala G, Yadav D, Upadhyay S, Ruddlesden-Popper phase A_2BO_4 oxides: Recent studies on structure, electrical, dielectric, and optical properties, J. Adv. Ceram., **9** (2020) 129–148. https://doi.org/10.1007/s40145-020-0365-x

2. Morales-Zapata MA, Larrea A, Laguna-Bercero MA, Lanthanide nickelates for their application on Solid Oxide Cells, Electrochim. Acta, **444** (2023) 141970. https://doi.org/10.1016/j.electacta.2023.141970

3. Ding P, Li W, Zhao H, et al., Review on Ruddlesden–Popper perovskites as cathode for solid oxide fuel cells, J. Phys. Mater., **4** (2021) 022002. https://doi.org/10.1088/2515-7639/abe392

4. Yatoo MA, Habib F, Malik AH, et al., Solid-oxide fuel cells: A critical review of materials for cell components, MRS Comm., **13** (2023) 378–384. https://doi.org/10.1557/s43579-023-00371-0

5. Wang Q, Fan H, Xiao Y, Zhang Y, Applications and recent advances of rare earth in solid oxide fuel cells, J Rare Earths, **40** (2022) 1668–1681. https://doi.org/10.1016/j.jre.2021.09.003

6. Manthiram A, Kim J-H, Kim YN, Lee K-T, Crystal chemistry and properties of mixed ionic-electronic conductors, J. Electroceram., **27** (2011) 93–107. https://doi.org/10.1007/s10832-011-9635-x

7. Antonova EP, Osinkin DA, Bogdanovich NM, et al., Electrochemical performance of $Ln_2NiO_{4+\delta}$ (Ln – La, Nd, Pr) and $Sr_2Fe_{1.5}Mo_{0.5}O_{6-\delta}$ oxide electrodes in contact with apatite-type $La_{10}(SiO_6)_4O_3$ electrolyte, Solid State Ion., **329** (2019) 82–89. https://doi.org/10.1016/j.ssi.2018.11.019

8. Antonova EP, Kolchugin AA, Pikalova EYu, et al., Development of electrochemically active electrodes for $BaCe_{0.89}Gd_{0.1}Cu_{0.01}O_{3-\delta}$ proton conducting electrolyte, Solid State Ion., **306** (2017) 55–61. https://doi.org/10.1016/j.ssi.2017.02.001

9. Sadykov VA, Sadovskaya EM, Eremeev NF, et al., Oxygen mobility in the materials for Solid Oxide Fuel cells and catalytic membranes (Review), Russ. J. Electrochem., **55** (2019) 701–718. https://doi.org/10.1134/S1023193519080147

10. Yang S, Liu G, Lee Y-L, et al., A systematic ab initio study of vacancy formation energy, diffusivity, and ionic conductivity of $Ln_2NiO_{4+\delta}$ (Ln=La, Nd, Pr), J. Power Sources, **576** (2023) 233200. https://doi.org/10.1016/j.jpowsour.2023.233200

11. Lee D, Lee H, Controlling oxygen mobility in Ruddlesden–Popper oxides, Materials, **10** (2017) 368. https://doi.org/10.3390/ma10040368

12. Chroneos A, Vovk RV, Goulatis IL, Goulatis LI, Oxygen transport in perovskite and related oxides: A brief review, J. Alloys Compd., **494** (2010) 190–195. https://doi.org/10.1016/j.jallcom.2010.01.071

13. Istomin SYa, Lyskov NV, Mazo GN, Antipov EV, Electrode materials based on complex d-metal oxides for symmetrical solid oxide fuel cells, Russ. Chem. Rev., **90** (2021) 644–676. https://doi.org/10.1070/RCR4979

14. Klyndyuk AI, Chizhova EA, Kharytonau DS, Medvedev DA, Layered oxygen-deficient double perovskites as promising cathode materials for solid oxide fuel cells, Materials, **15** (2021) 141. https://doi.org/10.3390/ma15010141

15. Tarutin AP, Lyagaeva JG, Medvedev DA, et al., Recent advances in layered $Ln_2NiO_{4+\delta}$ nickelates: Fundamentals and prospects of their applications in protonic ceramic fuel and electrolysis cells, J. Mater. Chem. A, **9** (2021) 154–195. https://doi.org/10.1039/d0ta08132a

16. Nikonov AV, Kuterbekov KA, Bekmyrza KZh, Pavzderin NB, A brief review of conductivity and thermal expansion of perovskite-related oxides for SOFC cathode, Euras. J. Phys. Funct. Mater., **2** (2018) 274–292. https://doi.org/10.29317/ejpfm.2018020309

17. Koval'chuk AN, Kuz'min AV, Osinkin DA, et al., Single SOFC with supporting Ni-YSZ anode, bilayer YSZ/GDC film electrolyte, and $La_2NiO_{4+\delta}$ cathode, Russ. J. Electrochem., **54** (2018) 541–546. https://doi.org/10.1134/S1023193518060101

18. Pikalova EYu, Bogdanovich NM, Kolchugin AA, et al., Electrical and electrochemical properties of $La_2NiO_{4+\delta}$-based cathodes in contact with $Ce_{0.8}Sm_{0.2}O_{2-\delta}$ electrolyte, Procedia Eng., **98** (2014) 105–110. https://doi.org/10.1016/j.proeng.2014.12.495

19. Antonova EP, Khodimchuk AV, Usov GR, et al., EIS analysis of electrode kinetics for $La_2NiO_{4+\delta}$ cathode in contact with $Ce_{0.8}Sm_{0.2}O_{1.9}$ electrolyte: from DRT analysis to physical model of the electrochemical process, J. Solid State Electrochem., **23** (2019) 1279–1287. https://doi.org/10.1007/s10008-019-04224-6

20. Antonova EP, Stroeva AYu, Tropin ES, Electrode performance of $La_2NiO_{4+\delta}$ cathodes in contact with $La_{0.9}Sr_{0.1}ScO_{3-\delta}$ proton-conducting oxide, J. Solid State Electrochem., **24** (2020) 1447–1451. https://doi.org/10.1007/s10008-020-04535-z

21. Antonova EP, Khodimchuk AV, Tropin ES, et al., Influence of modifying additives on electrochemical performance of $La_2NiO_{4+\delta}$ - based oxygen electrodes, Solid State Ion., **346** (2020) 115215. https://doi.org/10.1016/j.ssi.2019.115215

22. Tarutin AP, Lyagaeva JG, Farlenkov AS, et al., Cu-substituted $La_2NiO_{4+\delta}$ as oxygen electrodes for protonic ceramic electrochemical cells, Ceram. Int., **45** (2019) 16105–16112. https://doi.org/10.1016/j.ceramint.2019.05.127

23. Kovrova AI, Gorelov VP, Kuzmin AV, et al., Influence of $Ce_{0.8}R_{0.2}O_{2-a}$ (R = Y, Sm, Tb) submicron barrier layers at the $La_2NiO_{4+\delta}$/YSZ boundary on the electrochemical performance of a cathode, J. Solid State Electrochem., **25** (2021) 1789–1796. https://doi.org/10.1007/s10008-021-04942-w

24. Cherepanov VA, Gilev AR, Kiselev EA, Electrotransport in the La_2NiO_4-based solid solutions, Pure Appl. Chem., **91** (2019) 911–922. https://doi.org/10.1515/pac-2018-1001

25. Kol'chugin AA, Pikalova EYu, Bogdanovich NM, et al., Electrochemical properties of doped lantanum–nickelate-based electrodes, Russ. J. Electrochem., **53** (2017) 826–833. https://doi.org/10.1134/S1023193517080110

26. Pikalova E, Sadykov V, Sadovskaya E, et al., Correlation between structural and transport properties of Ca-doped La nickelates and their electrochemical performance, Crystals, **11** (2021) 297. https://doi.org/10.3390/cryst11030297

27. Xu S, Jacobs R, Morgan D, Factors controlling oxygen interstitial diffusion in the Ruddlesden–Popper oxide $La_{2-x}Sr_xNiO_{4+\delta}$, Chem. Mater. **30** (2018) 7166–7177. https://doi.org/10.1021/acs.chemmater.8b03146

28. Gilev AR, Kiselev EA, Zakharov DM, Cherepanov VA, Effect of calcium and copper/iron co-doping on defect-induced properties of La_2NiO_4-based materials, J. Alloys Compd., **753** (2018) 491–501. https://doi.org/10.1016/j.jallcom.2018.04.178

29. Antonova EP, Khodimchuk AV, Tropin ES, et al., Influence of polarization on the electrochemical activity of $La_{2-x}Ca_xNiO_{4+\delta}$ electrodes in contact with $Ce_{0.8}Sm_{0.2}O_{1.9}$ electrolyte, Int. J. Hydrogen Energy, **48** (2023) 22585–22593. https://doi.org/10.1016/j.ijhydene.2023.01.343

30. Sadykov VA, Sadovskaya EM, Pikalova EYu, et al., Transport features in layered nickelates: correlation between structure, oxygen diffusion, electrical and electrochemical properties, Ionics, **24** (2018) 1181–1193. https://doi.org/10.1007/s11581-017-2279-3

31. Türk H, Götsch T, Schmidt F, et al., Sr surface enrichment in solid oxide cells – approaching the limits of EDX analysis by multivariate statistical analysis and simulations, ChemCatChem, **14** (2022) e202200300. https://doi.org/10.1002/cctc.202200300

32. Wu X, Gu C, Cao J, et al., Investigations on electrochemical performance of $La_2NiO_{4+\delta}$ cathode material doped at A site for solid oxide fuel cells, Mater. Res. Express, **7** (2020) 065507. https://doi.org/10.1088/2053-1591/ab9c60

33. Gilev AR, Kiselev EA, Ozhiganov ME, Cherepanov VA, Factors governing surface exchange kinetics in undoped and strontium/iron co-substituted $La_2NiO_{4+\delta}$, Int. J. Hydrogen Energy, **48** (2023) 22573–22584. https://doi.org/10.1016/j.ijhydene.2023.01.182

34. Pikalova E, Eremeev N, Sadovskaya E, et al., Influence of the substitution with rare earth elements on the properties of layered lanthanum nickelate – Part I: Structure, oxygen transport and electrochemistry evaluation, Solid State Ion., **379** (2022) 115903. https://doi.org/10.1016/j.ssi.2022.115903

35. Pikalova E, Kolchugin A, Tsvinkinberg V, et al., Comprehensive study of functional properties and electrochemical performance of layered lanthanum nickelate substituted with rare-earth elements, J. Power Sources, **581** (2023) 233505. https://doi.org/10.1016/j.jpowsour.2023.233505

36. Li X, Benedek NA, Enhancement of ionic transport in complex oxides through soft lattice modes and epitaxial strain, Chem. Mater., **27** (2015) 2647–2652. https://doi.org/10.1021/acs.chemmater.5b00445

37. Gilev AR, Kiselev EA, Ozhiganov ME, Cherepanov VA, Polarization resistance of the Ruddlesden-Popper nickelates $La_{n+1}Ni_nO_{3n+1}$ (n = 1, 2, 3): Comparative analysis using the distribution of relaxation times method, Solid State Ion., **386** (2022) 116032. https://doi.org/10.1016/j.ssi.2022.116032

38. Flura A, Dru S, Nicollet C, et al., Chemical and structural changes in Ln_2NiO_4 (Ln=La, Pr or Nd) lanthanide nickelates as a function of oxygen partial pressure at high temperature, J. Solid State Chem., **228** (2015) 189–198. https://doi.org/10.1016/j.jssc.2015.04.029

39. Ruck K, Krabbes G, Vogel I, Structural and electrical properties of $La_{2-x}Ca_xNiO_{4+\delta}$ ($0 \le x < 0.4$) with regard to the oxygen content δ, Mat. Res. Bull., **34** (1999) 1689–1697. https://doi.org/10.1016/S0025-5408(99)00163-4

40. Jorgensen JD, Dabrowski B, Pei S, et al., Structure of the interstitial oxygen defect in $La_2NiO_{4+\delta}$, Phys. Rev. B, **40** (1989) 2187–2199. https://doi.org/10.1103/PhysRevB.40.2187

41. Choi SR, Lee J-I, Park H, et al., Multiple perovskite layered lanthanum nickelate Ruddlesden-Popper systems as highly active bifunctional oxygen catalysts, Chem. Eng. J., **409** (2021) 128226. https://doi.org/10.1016/j.cej.2020.128226

42. Tsvinkinberg VA, Tolkacheva AS, Filonova EA, et al., Structure, thermal expansion and electrical conductivity of $La_{2-x}Gd_xNiO_{4+\delta}$ ($0.0 \le x \le 0.6$) cathode materials for SOFC applications, J. Alloys Compd., **853** (2021) 156728. https://doi.org/10.1016/j.jallcom.2020.156728

43. Amira S, Ferkhi M, Khaled A, et al., Carbon-based lanthanum nickelate material $La_{2-x-y}Nd_xPr_yNiO_{4+\delta}$ (x = 0, 0.3, and 0.5; y = 0 and 0.2) as a bifunctional electrocatalyst for oxygen reduction in alkaline media, Ionics, **25** (2019) 3809–3822. https://doi.org/10.1007/s11581-019-02963-0

44. Boehm E, Bassat J, Dordor P, et al., Oxygen diffusion and transport properties in non-stoichiometric $Ln_{2-x}NiO_{4+\delta}$ oxides, Solid State Ion., **176** (2005) 2717–2725. https://doi.org/10.1016/j.ssi.2005.06.033

45. Sharma RK, Khamidy NI, Bassat JM, Djurado E, $La_{2-x}Pr_xNiO_{4+\delta}$-based efficient SOFC cathodes: Effect of microstructure, composition and architecture, ECS Trans., **78** (2017) 581–591. https://doi.org/10.1149/07801.0581ecst

46. Kolchugin AA, Pikalova EYu, Bogdanovich NM, et al., Structural, electrical and electrochemical properties of calcium-doped lanthanum nickelate, Solid State Ion., **288** (2016) 48–53. https://doi.org/10.1016/j.ssi.2016.01.035

47. Naumovich EN, Kharton VV, Atomic-scale insight into the oxygen ionic transport mechanisms in La_2NiO_4-based materials, J. Mol. Struct., **946** (2010) 57–64. https://doi.org/10.1016/j.theochem.2009.12.003

48. Minervini L, Grimes RW, Kilner JA, Sickafus KE, Oxygen migration in $La_2NiO_{4+\delta}$, J. Mater. Chem., **10** (2000) 2349–2354. https://doi.org/10.1039/b004212i

49. Chroneos A, Parfitt D, Kilner JA, Grimes RW, Anisotropic oxygen diffusion in tetragonal $La_2NiO_{4+\delta}$: molecular dynamics calculations, J. Mater. Chem., **20** (2010) 266–270. https://doi.org/10.1039/B917118E

50. Li X, Huan D, Shi N, et al., Defects evolution of Ca doped $La_2NiO_{4+\delta}$ and its impact on cathode performance in proton-conducting solid oxide fuel cells, Int. J. Hydrogen Energy, **45** (2020) 17736–17744. https://doi.org/10.1016/j.ijhydene.2020.04.150

51. Skinner S, Oxygen diffusion and surface exchange in $La_{2-x}Sr_xNiO_{4+\delta}$, Solid State Ion., **135** (2000) 709–712. https://doi.org/10.1016/S0167-2738(00)00388-X

52. Tropin ES, Ananyev MV, Farlenkov AS, et al., Surface defect chemistry and oxygen exchange kinetics in $La_{2-x}Ca_xNiO_{4+\delta}$, J. Solid State Chem., **262** (2018) 199–213. https://doi.org/10.1016/j.jssc.2018.03.020

53. Pikalova EYu, Kolchugin AA, Sadykov VA, et al., Structure, transport properties and electrochemical behavior of the layered lanthanide nickelates doped with calcium, Int. J. Hydrogen Energy, **43** (2018) 17373–17386. https://doi.org/10.1016/j.ijhydene.2018.07.115

54. Gauquelin N Impact of the structural anisotropy of $La_2NiO_{4+\delta}$ on high temperature surface modifications and diffusion of oxygen [Doctorale Science Theses] Rennes (France): Universite De Rennes; 2010. 226 p. http://publications.rwth-aachen.de/record/82802/files/3662.pdf

55. Bassat J, Anisotropic ionic transport properties in $La_2NiO_{4+\delta}$ single crystals, Solid State Ion., **167** (2004) 341–347. https://doi.org/10.1016/j.ssi.2003.12.012

56. Matsuda M, Hashimoto M, Matsunaga C, et al., Electrophoretic fabrication of a-b plane oriented La_2NiO_4 cathode onto electrolyte in strong magnetic field for low-temperature operating solid oxide fuel cell, J. Eur. Ceram. Soc., **36** (2016) 4077–4082. https://doi.org/10.1016/j.jeurceramsoc.2016.06.043

57. Shin J, Yang S, Ji H-I, et al., Low-temperature processing technique of Ruddlesden-Popper cathode for high-performance solid oxide fuel cells, J. Alloys Compd., **868** (2021) 159092. https://doi.org/10.1016/j.jallcom.2021.159092

58. Inprasit T, Limthongkul P, Wongkasemjit S, Sol-gel and solid-state synthesis and property study of $La_{2-x}Sr_xNiO_4$ ($x \leq 0.8$), J. Electrochem. Soc., **157** (2010) B1726. https://doi.org/10.1149/1.3489262

59. Lyagaeva J, Medvedev D, Pikalova E, et al., A detailed analysis of thermal and chemical compatibility of cathode materials suitable for $BaCe_{0.8}Y_{0.2}O_{3-\delta}$ and $BaZr_{0.8}Y_{0.2}O_{3-\delta}$ proton electrolytes for solid oxide fuel cell application, Int. J. Hydrogen Energy, **42** (2017) 1715–1723. https://doi.org/10.1016/j.ijhydene.2016.07.248

60. Sameshima S, Kawaminami M, Hirata Y, Thermal expansion of rare-earth-doped ceria ceramics, J. Ceram. Soc. Japan, **110** (2002) 597–600. https://doi.org/10.2109/jcersj.110.597

61. Stevenson JW, Hasinska K, Canfield NL, Armstrong TR, Influence of cobalt and iron additions on the electrical and thermal properties of $(La,Sr)(Ga,Mg)O_{3-\delta}$, J. Electrochem. Soc., **147** (2000) 3213. https://doi.org/10.1149/1.1393885

62. Shaula A, Kharton V, Marques F, Ionic and electronic conductivities, stability and thermal expansion of $La_{10-x}(Si,Al)_6O_{26\pm\delta}$ solid electrolytes, Solid State Ion., **177** (2006) 1725–1728. https://doi.org/10.1016/j.ssi.2005.11.023

63. Pikalova EYu, Kolchugin AA, The influence of the substituting element (M = Ca, Sr, Ba) in $La_{1.7}M_{0.3}NiO_{4+\delta}$ on the electrochemical performance of the composite electrodes, Eur. Chem.-Tech. J., **18** (2016) 3. https://doi.org/10.18321/ectj386

64. Lesnichyova A, Stroeva A, Belyakov S, et al., Water uptake and transport properties of $La_{1-x}Ca_xSc_cO_{3-\alpha}$ proton-conducting oxides, Materials, **12** (2019) 2219. https://doi.org/10.3390/ma12142219

65. Hernández AM, Mogni L, Caneiro A, $La_2NiO_{4+\delta}$ as cathode for SOFC: Reactivity study with YSZ and CGO electrolytes, Int. J. Hydrogen Energy, **35** (2010) 6031–6036. https://doi.org/10.1016/j.ijhydene.2009.12.077

66. Philippeau B, Mauvy F, Mazataud C, et al., Comparative study of electrochemical properties of mixed conducting $Ln_2NiO_{4+\delta}$ (Ln=La, Pr and Nd) and $La_{0.6}Sr_{0.4}Fe_{0.8}Co_{0.2}O_{3-\delta}$ as SOFC cathodes associated to $Ce_{0.9}Gd_{0.1}O_{2-\delta}$, $La_{0.8}Sr_{0.2}Ga_{0.8}Mg_{0.2}O_{3-\delta}$ and $La_9Sr_1Si_6O_{26.5}$ electrolytes, Solid State Ion., **249–250** (2013) 17–25. https://doi.org/10.1016/j.ssi.2013.06.009

67. Taş AC, Majewski PJ, Aldinger F, Chemical preparation of pure and strontium- and/or magnesium-doped lanthanum gallate powders, J. Am. Ceram. Soc., **83** (2000) 2954–2960. https://doi.org/10.1111/j.1151-2916.2000.tb01666.x

68. Maglia F, Anselmi-Tamburini U, Chiodelli G, et al., Electrical, structural, and microstructural characterization of nanometric $La_{0.9}Sr_{0.1}Ga_{0.8}Mg_{0.2}O_{3-\delta}$ (LSGM) prepared by high-pressure spark plasma sintering, Solid State Ion., **180** (2009) 36–40. https://doi.org/10.1016/j.ssi.2008.10.005

69. Kesapragada SV, Bhaduri SB, Bhaduri S, Singh P, Densification of LSGM electrolytes using activated microwave sintering, J. Power Sources, **124** (2003) 499–504. https://doi.org/10.1016/j.jpowsour.2003.06.002

70. Song J, Ning D, Boukamp B, et al., Structure, electrical conductivity and oxygen transport properties of Ruddlesden–Popper phases $Ln_{n+1}Ni_nO_{3n+1}$ (Ln = La, Pr and Nd; n = 1, 2 and 3), J. Mater. Chem. A, **8** (2020) 22206–22221. https://doi.org/10.1039/D0TA06731H

71. Lou Z, Dai N, Wang Z, et al., Preparation and electrochemical characterization of Ruddlesden–Popper oxide $La_4Ni_3O_{10}$ cathode for IT-SOFCs by sol–gel method, J. Solid State Electrochem., **17** (2013) 2703–2709. https://doi.org/10.1007/s10008-013-2150-z

72. Pikalova E, Kolchugin A, Zakharchuk K, et al., Mixed ionic-electronic conductivity, phase stability and electrochemical activity of Gd-substituted $La_2NiO_{4+\delta}$ as oxygen electrode material for solid oxide fuel/electrolysis cells, Int. J. Hydrogen Energy, **46** (2021) 16932–16946. https://doi.org/10.1016/j.ijhydene.2021.03.007

73. Nakamura T, Yashiro K, Sato K, Mizusaki J, Electronic state of oxygen nonstoichiometric $La_{2-x}Sr_xNiO_{4+\delta}$ at high temperatures, Phys. Chem. Chem. Phys., **11** (2009) 3055. https://doi.org/10.1039/b823364k

74. Shaula AL, Naumovich EN, Viskup AP, et al., Oxygen transport in $La_2NiO_{4+\delta}$: Assessment of surface limitations and multilayer membrane architectures, Solid State Ion., **180** (2009) 812–816. https://doi.org/10.1016/j.ssi.2009.01.005

75. Goodenough JB, Ramasesha S, Further evidence for the coexistence of localized and itinerant 3d electrons in La_2NiO_4, Mat. Res. Bull., **17** (1982) 383–390. https://doi.org/10.1016/0025-5408(82)90089-7

76. Goodenough JB, Bond-length mismatch in intergrowth structures, J. Less Common Met., **116** (1986) 83–93. https://doi.org/10.1016/0022-5088(86)90219-5

77. Bassat JM, Odier P, Loup JP, The Semiconductor-to-Metal Transition in Question in $La_{2-x}NiO_{4+\delta}$ ($\delta > 0$ or $\delta < 0$), J. Solid State Chem., **110** (1994) 124–135. https://doi.org/10.1006/jssc.1994.1146

78. Nishiyama S, Sakaguchi D, Hattori T, Electrical conduction and thermoelectricity of $La_2NiO_{4+\delta}$ and $La_2(Ni,Co)O_{4+\delta}$, Solid State Comm., **94** (1995) 279–282. https://doi.org/10.1016/0038-1098(95)00062-3

79. Vashook VV, Tolochko SP, Yushkevich II, et al., Oxygen nonstoichiometry and electrical conductivity of the solid solutions $La_{2-x}Sr_xNiO_y$ ($0 \le x \le 0.5$), Solid State Ion., **110** (1998) 245–253. https://doi.org/10.1016/S0167-2738(98)00134-9

80. Ananyev MV, Tropin ES, Eremin VA, et al., Oxygen isotope exchange in $La_2NiO_{4\pm\delta}$, Phys. Chem. Chem. Phys., **18** (2016) 9102–9111. https://doi.org/10.1039/C5CP05984D

81. Zhao K, Wang Y-P, Chen M, et al., Electrochemical evaluation of $La_2NiO_{4+\delta}$ as a cathode material for intermediate temperature solid oxide fuel cells, Int. J. Hydrogen Energy, **39** (2014) 7120–7130. https://doi.org/10.1016/j.ijhydene.2014.02.106

82. Lee Y, Kim H, Electrochemical performance of $La_2NiO_{4+\delta}$ cathode for intermediate-temperature solid oxide fuel cells, Ceram. Int., **41** (2015) 5984–5991. https://doi.org/10.1016/j.ceramint.2015.01.037

83. Kim SJ, Kim KJ, Dayaghi AM, Choi GM, Polarization and stability of $La_2NiO_{4+\delta}$ in comparison with $La_{0.6}Sr_{0.4}Co_{0.2}Fe_{0.8}O_{3-\delta}$ as air electrode of solid oxide electrolysis cell, Int. J. Hydrogen Energy, **41** (2016) 14498–14506. https://doi.org/10.1016/j.ijhydene.2016.05.284

84. Ogier T, Mauvy F, Bassat J-M, et al., Overstoichiometric oxides $Ln_2NiO_{4+\delta}$ (Ln = La, Pr or Nd) as oxygen anodic electrodes for solid oxide electrolysis application, Int. J. Hydrogen Energy, **40** (2015) 15885–15892. https://doi.org/10.1016/j.ijhydene.2015.09.107

85. Yoo Y-S, Choi M, Hwang J-H, et al., $La_2NiO_{4+\delta}$ as oxygen electrode in reversible solid oxide cells, Ceram. Int., **41** (2015)6448–6454. https://doi.org/10.1016/j.ceramint.2015.01.083

86. Filonova E, Pikalova E, Overview of approaches to increase the electrochemical activity of conventional perovskite air electrodes, Materials, **16** (2023) 4967. https://doi.org/10.3390/ma16144967

87. Vibhu V, Suchomel MR, Penin N, et al., Structural transformations of the $La_{2-x}Pr_xNiO_{4+\delta}$ system probed by high-resolution synchrotron and neutron powder diffraction, Dalton Trans, **48** (2019) 266–277. https://doi.org/10.1039/C8DT03524E

88. Sadykov VA, Pikalova EYu, Kolchugin AA, et al., Oxygen transport properties of Ca-doped Pr_2NiO_4, Solid State Ion., **317** (2018) 234–243. https://doi.org/10.1016/j.ssi.2018.01.035

89. Khamidy NI, Laurencin J, Ferreira Sanchez D, et al., Durability of nanostructured $LaPrNiO_{4+\delta}$ electrode for solid oxide cells: Electrochemical, microstructural, and structural investigation, J. Power Sources, **450** (2020) 227724. https://doi.org/10.1016/j.jpowsour.2020.227724

90. Vibhu V, Flura A, Rougier A, et al., Electrochemical ageing study of mixed lanthanum/praseodymium nickelates $La_{2-x}Pr_xNiO_{4+\delta}$ as oxygen electrodes for solid oxide fuel or electrolysis cells, J. Energy Chem., **46** (2020) 62–70. https://doi.org/10.1016/j.jechem.2019.10.012

91. Kim GT, Jacobson AJ, Electrochemical characterization of $La_{2-x}Pr_xNiO_{4+x}$ for application as cathodes in intermediate temperature SOFCs, MRS Proc., **972** (2006) 0972-AA11-04. https://doi.org/10.1557/PROC-0972-AA11-04

92. Zhao C, Zhou Q, Zhang T, et al., Preparation and electrochemical properties of $La_{1.5}Pr_{0.5}NiO_4$ and $La_{1.5}Pr_{0.5}Ni_{0.9}Cu_{0.1}O_4$ cathode materials for intermediate-temperature solid oxide fuel cells, Mat. Res. Bull., **113** (2019) 25–30. https://doi.org/10.1016/j.materresbull.2019.01.016

93. Nishimoto S, Takahashi S, Kameshima Y, et al., Properties of $La_{2-x}Pr_xNiO_4$ cathode for intermediate-temperature solid oxide fuel cells, J. Ceram. Soc. Japan, **119** (2011) 246–250. https://doi.org/10.2109/jcersj2.119.246

94. Sharma RK, Celikbilek O, Burriel M, et al., Electrochemical performance and chemical stability of architecturally designed $La_{2-x}Pr_xNiO_{4+\delta}$ IT-SOFC cathodes, ECS Trans., **72** (2016) 1–8. https://doi.org/10.1149/07233.0001ecst

95. Usenka A, Pankov V, Vibhu V, et al., Temperature programmed oxygen desorption and sorption processes on $Pr_{2-x}La_xNiO_{4+\delta}$ nickelates, ECS Trans., **91** (2019) 1341–1353. https://doi.org/10.1149/09101.1341ecst

96. Druce J, Kilner JA, Ishihara T, Relating Electrochemical performance measurements and surface analyses of $Pr_{2-x}La_xNiO_{4+\delta}$ electrode materials, ECS Trans., **57** (2013) 3269–3276. https://doi.org/10.1149/05701.3269ecst

97. Zhang Y, Wang W, Wang Y, et al., Role of Pr-vacancies and O-interstitials on the activity and stability of $(Pr_{1-x}Ln_x)_2NiO_4$ (Ln = La, Nd, Pm, Sm, Gd, Tb, Dy, and Ho) towards oxygen reduction reactions: A DFT study, J. Electrochem. Soc., **168** (2021) 124508. https://doi.org/10.1149/1945-7111/ac4057

98. Vibhu V, Rougier A, Nicollet C, et al., $La_{2-x}Pr_xNiO_{4+\delta}$ as suitable cathodes for metal supported SOFCs, Solid State Ion., **78** (2015) 32–37. https://doi.org/10.1016/j.ssi.2015.05.005

99. Ishikawa H, Toyosumi Y, Ishikawa K, Structural phase transition of $La_{2-x}Nd_xNiO_{4+\delta}$ ($0.0 \le x \le 2.0$), J. Alloys Compd., **408–412** (2006) 1196–1199. https://doi.org/10.1016/j.jallcom.2004.12.143

100. Pikalov SM, Vedmid' LB, Filonova EA, et al., High-temperature behavior of calcium substituted layered neodymium nickelates, J. Alloys Compd., **801** (2019) 558–567. https://doi.org/10.1016/j.jallcom.2019.05.349

101. Wan J, Goodenough J, Zhu J, $Nd_{2-x}La_xNiO_{4+\delta}$, a mixed ionic/electronic conductor with interstitial oxygen, as a cathode material, Solid State Ion., **178** (2007) 281–286. https://doi.org/10.1016/j.ssi.2007.01.013

102. Amow G, Skinner SJ, Recent developments in Ruddlesden–Popper nickelate systems for solid oxide fuel cell

cathodes, J. Solid State Electrochem., **10** (2006) 538–546. https://doi.org/10.1007/s10008-006-0127-x

103. Garali M, Kahlaoui M, Mohammed B, et al., Synthesis, characterization and electrochemical properties of $La_{2-x}Eu_xNiO_{4+\delta}$ Ruddlesden-Popper-type layered nickelates as cathode materials for SOFC applications, Int. J. Hydrogen Energy, **44** (2019) 11020–11032. https://doi.org/10.1016/j.ijhydene.2019.02.158

104. Sadykov VA, Sadovskaya EM, Filonova EA, et al., Oxide ionic transport features in Gd-doped La nickelates, Solid State Ion., **357** (2020) 115462. https://doi.org/10.1016/j.ssi.2020.115462

105. Wu CH, Shi YJ, Lu F, et al., Ruddlesden–Popper-type $La_{1.5-x}Eu_xPr_{0.5}Ni_{0.9}Cu_{0.1}O_{4+\delta}$ as a potential cathode material for H-SOFCs, Phys. Solid State, **63** (2021) 775–784. https://doi.org/10.1134/S1063783421050218

106. Vegard L, Die konstitution der mischkristalle und die raumfllung der atome, Z Physik, **5** (1921) 17–26. https://doi.org/10.1007/BF01349680

107. Guseva EM, Ivanov RA, Pikalova EYu, Filonova EA, Modeling of crystal structure parameters in complex-oxide perovskite-like systems. In: Materials of the XIX Russian Conference «Physical Chemistry and Electrochemistry of molten and solid electrolytes»; 2023 Sep 17-21; Ekaterinburg, Russia. p. 188. http://conference.ihte2023.tilda.ws/sbornik

108. Choisnet J, Structure and bonding anisotropy in intergrowth oxides: A clue to the manifestation of bidimensionality in T-, T'-, and T*-type structures, J. Solid State Chem., **147** (1999) 379–389. https://doi.org/10.1006/jssc.1999.8381

109. Shannon RD, Revised effective ionic radii and systematic studies of interatomic distances in halides and chalcogenides, Acta Cryst. A, **32** (1976) 751–767. https://doi.org/10.1107/S0567739476001551

110. Goldschmidt VM, Die gesetze der krystallochemie, Naturwissenschaften, **14** (1926) 477–485. https://doi.org/10.1007/BF01507527

111. Ganguly P, Rao CNR, Crystal chemistry and magnetic properties of layered metal oxides possessing the K_2NiF_4 or related structures, J. Solid State Chem., **53** (1984) 193–216. https://doi.org/10.1016/0022-4596(84)90094-X

112. Vibhu V, Rougier A, Nicollet C, et al., $La_{2-x}Pr_xNiO_{4+\delta}$ as suitable cathodes for metal supported SOFCs, Solid State Ion., **278** (2015)32–37. https://doi.org/10.1016/j.ssi.2015.05.005

113. Guseva EM, Pikalova EYu, Tsvinkinberg VA, et al Crystal structure and physico-chemical properties of $La_{2-x}Sm_xNiO_{4+\delta}$ solid solutions. In: Abstracts of the XXXII Russian Youth Scientific Conference with International Participation Problems of Theoretical and Experimental Chemistry; 2022 Apr 19-22; Ekaterinburg, Russia. p. 162. http://hdl.handle.net/10995/117133

114. Kharton VV, Kovalevsky AV, Avdeev M, et al., Chemically induced expansion of $La_2NiO_{4+\delta}$-based materials, Chem. Mater., **19** (2007) 2027–2033. https://doi.org/10.1021/cm070096x

115. Kharton VV, Yaremchenko AA, Shaula AL, et al., Transport properties and stability of Ni-containing mixed conductors with perovskite- and K_2NiF_4-type structure, J. Solid State Chem., **177** (2004) 26–37. https://doi.org/10.1016/S0022-4596(03)00261-5

116. Chaker H, Raies I, Chouket A, et al., Chemical and physical characterizations of the n = 1 Ruddlesden–Popper phases: $Nd_{2-y}Sr_yNi_{1-x}Co_xO_{4\pm\delta}$ (y = 1 and $0.1 \le x \le 0.9$), Ionics, **23** (2017) 2229–2240. https://doi.org/10.1007/s11581-017-2167-x

117. Shen Y, Zhao H, Liu X, Xu N, Preparation and electrical properties of Ca-doped $La_2NiO_{4+\delta}$ cathode materials for IT-SOFC, Phys. Chem. Chem. Phys., **12** (2010) 15124. https://doi.org/10.1039/c0cp00261e

118. Zakharchuk K, Kovalevsky A, Yaremchenko A, Characterization of Ruddlesden-Popper $La_{2-x}Ba_xNiO_{4\pm\delta}$ nickelates as potential electrocatalysts for solid oxide cells, Materials, **16** (2023) 1755. https://doi.org/10.3390/ma16041755

119. Bo G Oxygen reduction kinetics of $La_{2-x}Sr_xNiO_{4+\delta}$ electrodes for solid oxide fuel cells [Graduate Theses]. Morgantown (USA): West Virginia University; 2016. 58 p. https://researchrepository.wvu.edu/cgi/viewcontent.cgi?article=6759&context=etd

120. Aguadero A, Escudero MJ, Pérez M, et al., Effect of Sr content on the crystal structure and electrical properties of the system $La_{2-x}Sr_xNiO_{4+\delta}$ ($0 \le x \le 1$), Dalton Trans., **36** (2006) 4377–4383. https://doi.org/10.1039/B606316K

121. Hildenbrand N, Nammensma P, Blank DHA, et al., Influence of configuration and microstructure on performance of $La_2NiO_{4+\delta}$ intermediate-temperature solid oxide fuel cells cathodes, J. Power Sources, **238** (2013) 442–453. https://doi.org/10.1016/j.jpowsour.2013.03.192

122. Escudero MJ, Aguadero A, Alonso JA, Daza L, A kinetic study of oxygen reduction reaction on La_2NiO_4 cathodes by means of impedance spectroscopy, J. Electroanal. Chem., **611** (2007) 107–116. https://doi.org/10.1016/j.jelechem.2007.08.006

123. Nicollet C, Flura A, Vibhu V, et al., $La_2NiO_{4+\delta}$ infiltrated into gadolinium doped ceria as novel solid oxide fuel cell cathodes: Electrochemical performance and impedance modelling, J. Power Sources, **294** (2015) 473–482. https://doi.org/10.1016/j.jpowsour.2015.06.077

124. Kim GT, Wang S, Jacobson AJ, et al., Impedance studies of dense polycrystalline thin films of $La_2NiO_{4+\delta}$, J. Mater. Chem., **17** (2007) 1316. https://doi.org/10.1039/b616101d

125. Ghamarinia M, Babaei A, Zamani C, Aslannejad H, Application of the distribution of relaxation time method in electrochemical analysis of the air electrodes in the SOFC/SOEC devices: A review, Chem. Eng. J. Adv., **15** (2023) 100503. https://doi.org/10.1016/j.ceja.2023.100503

126. Mauvy F, Lalanne C, Bassat J-M, et al., Electrode properties of $Ln_2NiO_{4+\delta}$ (Ln=La, Nd, Pr), J. Electrochem. Soc., **153** (2006) A1547. https://doi.org/10.1149/1.2207059

127. Adler S, Limitations of charge-transfer models for mixed-conducting oxygen electrodes, Solid State Ion., **135** (2000) 603–612. https://doi.org/10.1016/S0167-2738(00)00423-9

128. Lu Y, Kreller C, Adler SB, Measurement and modeling of the impedance characteristics of porous $La_{1-x}Sr_xCoO_{3-\delta}$ electrodes, J. Electrochem. Soc., **156** (2009) B513. https://doi.org/10.1149/1.3079337

129. Ascolani-Yael J, Montenegro-Hernández A, Garcés D, et al., The oxygen reduction reaction in solid oxide fuel cells: from kinetic parameters measurements to electrode design, J.

Phys. Energy, **2** (2020) 042004. https://doi.org/10.1088/2515-7655/abb4ec

130. Chiu T-W, Lin M-X, Shih H-Y, et al., Preparation and performance of $PrLaNiO_4$ and $(La_{0.75}Sr_{0.2}Ba_{0.05})_{0.175}Ce_{0.825}O_{1.891}$ composite cathode material by solid state reaction for IT-SOFCs, Ceram. Int., **43** (2017) S700–S704. https://doi.org/10.1016/j.ceramint.2017.05.269